Научно веће
Институт за физику
Београд

МОЛБА

Молим Научно веће Института за физику у Београду да покрене мој реизбор у звање **истраживач сарадник**, а на основу приложене документације:

1. Потписани захтев кандидата за покретање поступка.
2. Мишљење руководиоца пројекта са предлогом комисије која ће писати извештај. Комисија треба да се састоји од најмање три члана у научном или наставном звању, при чему бар један није запослен у нашем Институту, а бар половина јесте запослена код нас.
3. Кратка стручна биографија кандидата (до 1 стране).
4. Кратак преглед научне активности кандидата (до 1 стране).
5. Списак објављених радова и других публикација, разврстан по важећим категоријама прописаним Правилником.
6. Копије објављених радова и других публикација (верзије из часописа, зборника апстраката, итд.).
7. Потврда о уписаним докторским студијама .
8. Потврда о просеку на основним и мастер студијама (диплома или уверење о дипломирању), који мора бити већи од 8.
9. Потврда о прихваћеној теми докторске дисертације.

У Београду,   Подносилац молбе
31.08.2018. године   _Ивана Ђуришић_
                                                                    Ивана Ђуришић

Научно веће
Институт за физику
Београд

Датум:
Београд, 31. август 2018. год.

Предмет:
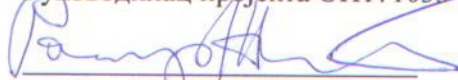**Мишљење руководиоца пројекта за реизбор Иване Ђуришић у звање истраживач сарадник**

Ивана Ђуришић је докторске студије на Физичком факултету Универзитета у Београду уписала је 2008/2009. године и од 1.октобра 2008. запослена је на Институту за физику. У периоду 2009. до 2010. године била је ангажована на међународном FP7 пројекту „Nano Tools for Ultra Fast Dna Sequencing". Од јануара 2011. године ангажована је на пројектима основних истраживања ОИ171033 „Електронске, транспортне и оптичке особине нанофазних материјала" и интердисциплинарних истраживања ИИИ41028 „Интегрална студија идентификације регионалних генетских фактора ризика и фактора ризика животне средине за масовне незаразне болести хумане популације у Србији" Министарства просвете, науке и технолошког развоја.

Резултати досадашњег истраживачког рада колегинице Ђуришић публиковани су у водећем међународном часопису. До сада постигнути резултати колегинице Ђуришић показују да поседује квалитете неопходне за бављење научно-истраживачким радом. С обзиром да колегиница испуњава све критеријуме прописане од стране Министарства просвете, науке и технолошког развоја сагласан сам с покретањем поступка за реизбор Иване Ђуришић у звање истраживач сарадник.

За састав Комисије за реизбор Иване Ђуришић у звање истраживач сарадник предлажем:

1. др Радомир Жикић, научни саветник Институт за физику, Београд
2. др Милош Дражић научни сарадник, Институт за физику, Београд
3. др Жељко Шљиванчанин, научни саветник, Институт за нуклеарне науке Винча, Београд

Руководилац пројекта ОИ171033

др Радомир Жикић,
научни саветник,
Институт за физику, Београд

СТРУЧНА БИОГРАФИЈА

Образовање:

Ивана Ђуришић је рођена 30. августа 1980. године у Беранама, Република Црна Гора, где је завршила Основну школу и Гимназију.

Уписала је студије физике на Природно математичком факултету, Универзитета у Подгорици школске 1999/2000. године, где је завршила прву годину студија.

Другу годину студија уписала је на Физичком факултету, Универзитета у Београду школске 2000/2001. године, смер Теоријска и експериментална физика. Дипомирала је 2005. године и стекла звање дипломирани физичар са просечном оценом 9.07 у току студија. Дипломски рад под називом „Фотонски кристали у микроталасном подручју" урадила је на Институту за физику под менторством др Радомира Жикића.

Као студент магистарских стидија у периоду од 2005-2008. године била је стипендиста Министарства за науку и заштиту животне средине Републике Србије

Докторске студије уписала је школске 2008/2009. године на Физичком факултету, Универзитета у Београду из области Квантна, математичка и нанофизика

Радно искуство:

Од 2005-2008. године била је ангажована на пројекту основних истраживања 141029А „Динамика атомских, молекулских и мезоскопских система" реализованом на Институту за физику под руководством др Таска Грозданова. Од 1. октобра 2008. године запослена је као истраживач приправник.

Од 2009-2010. године била је ангажована на међународном пројекту FP7-NMP „Nano Tools for Ultra Fast DNA Sequencing" под руководством др Радомира Жикића.

Од јануара 2010. ангажована је на пројекту основних истраживања 171033 „Електронске, транспортне и оптичке особине нанофазних материјала" реализованом на Институту за физику под руководством др Радомира Жикћа и на пројекту интердисциплинарних истраживања 41028 „Интегрална студија идентификације регионалних генетских фактора ризика и фактора ризика животне средине на незаразне болести људске популације у Србији".

.

Научна активност кандидата

Област истраживања Иване Ђуришић је физика кондензованог стања материје, посебно област квантног електронског транспорта кроз наноструктуре у неравнотежном режиму. У раду користи нумеричке методе које се ослањају на DFT (density functional theory) кодовима уз коришћење формализма неравнотежних Гринових функција (NEGF- non-equilibrium Green's function).

Основни системи који су у фокусу истраживања и рада на докторској тези су DNA нуклеотиди између две електроде на задатом напону. Пронађене су разлике у транспортним карактеристикама (трансмисија, струја тунелирања, положаји HOMO и LUMO енергетских нивоа..) кроз поједине DNA нуклеотиде, што омогућава њихово лакше препознавање. Теорија функционала густине (DFT) је ab initio метод и даје електронску густину и укупну енергију система коритећи апроксимативни облик изменско корелационог функционала као што су B3LYP (Becke, 3-parameter, Lee-Yang-Parr approximation), LDA (local-density approximation) или GGA (generalized gradient approximation) помоћу програмских пакета Siesta, TranSIESTA, TBTrans и NWChem који, тестирани на системима са великим бројем атома, дају одличне разултате у великом броју примена. Такође, изучаване су особине оваквих система у зависности од оријентације нуклеотида у односу на електроде за које је предложен протокол секвенцирања.

У свом раду докторант је испитивао и електронске и вибрационе особине органских молекула TPD (N,N′-bis(3-methylphenyl)-N,N′-bis(phenyl)benzedine) и DPVBi (4,4′-Bis(2,2-diphenylvinyl)-1,1′-biphenyl) и њихових оксидованих врста, такође у оквиру теорије функционала густине. Показао је да се резултати за TPD и DPVBi молекуле који су добијени помоћу DFT формализма веома добро слажу са експерименталним оптичким феноменима који се уочавају у слојевима чистих и оксидованих TPD и DPVBi филмова. Теоријски добијени резултати за вибрационе спектре се добро слажу са њиховим експерименталним инфрацрвеним спектрима. Такође разматрано је понашање у графену услед бушења материјала помоћу златног типа. Теоријски резултати су показали да ће се различити дефекти појавити зависно од места бушења у бентеновом прстену. Такође разлике ће се уочити за различите облике типа. Уведен је концепт SPM (scanning probe microscopy) са типом који ротира као могућност за будуће експерименте у овој области.

Ивана Ђуришић је показала висок степен самосталности у истраживачком раду. Резултати су публиковани у три рада, два рада у међународним часописима категорије М21 и један рад у домаћем часопису категорије М51.

Списак научних радова и саопштења
Научни радови:

Fast photoluminescence quenching in thin films of 4,4'-bis(2,2-diphenylvinyl)-1,1'-biphenyl exposed to air
A.Ž.Tomović, V.P.Jovanović, **I.Đurišić**, V.Z.Cerovski, B.Nastasijević, S.R.Veličković, K.Radulović, R.Žikić
прихваћен за публикацију у Journal of luminescence (2015)
DOI:10.1016/j.jlumin.2015.06.036
M21, IF(2014)=2.719

Designing topological defects in 2D materials using scanning probe microscopy and a self-healing mechanism: A density functional-based molecular dynamics study
Igor Popov, **I. Đurišić**, Milivoj Belić
прихваћен за публикацију у Nanotechnology (2017)
DOI: 10.1088/1361-6528/aa9679
M21, IF(2017)= 3.404

Fast photoluminescence quenching in thin films of 4,4′-bis(2,2-diphenylvinyl)-1,1′-biphenyl exposed to air

A.Ž. Tomović [a], V.P. Jovanović [b,*], I. Đurišić [a], V.Z. Cerovski [a], B. Nastasijević [c], S.R. Veličković [c], K. Radulović [d], R. Žikić [a]

[a] Institute of Physics, University of Belgrade, Pregrevica 118, 11000 Belgrade, Serbia
[b] Institute for Multidisciplinary Research, University of Belgrade, Kneza Višeslava 1, 11000 Belgrade, Serbia
[c] Vinča Institute of Nuclear Sciences, University of Belgrade, P.O. Box 522, 11001 Belgrade, Serbia
[d] Institute of Chemistry, Technology and Metallurgy, University of Belgrade, Njegoševa 12, 11000 Belgrade, Serbia

ABSTRACT

The photoluminescence (PL) quenching mechanism of UV light and air-exposed amorphous thin films of 4,4′-bis(2,2-diphenylvinyl)-1,1′-biphenyl (DPVBi), a well-known hole-transport material used in organic light-emitting diodes, is studied. Thin films of DPVBi are stable when exposed to UV light in vacuum but tend to degrade if oxygen is present simultaneously. This is evident from the changes in UV–vis absorption spectra of the latter, showing that degradation rate of DPVBi films is linearly proportional to both oxygen concentration and UV light intensity. Mass spectrometry study of such films revealed a number of different oxygen-containing molecules and fragments of DPVBi thus confirming apparent photo-oxidation process. Also, DFT study of molecular DPVBi with and without oxygen was carried out, the IR spectra calculated for the lowest energy molecules found and the results are compared with the experiment. The most sensitive to photo-oxidation is DPVBi photoluminescence, which decays exponentially with respect to the concentration of photo-oxidized DPVBi molecules (impurities). The PL quantum yield of DPVBi thin film drops to a half of its original value for 0.2% of the impurities present, at which point an average distance between DPVBi molecules (the donors) and photo-oxidized DPVBi species (acceptors) is an order of magnitude larger than the separation between two adjacent molecules. This implies a need for a long-range Förster energy transfer, which we rule out based on the lack of a donor–acceptor spectral overlap. The apparent discrepancy can be removed by postulating exciton self-diffusion in DPVBi thin films, for which there is supporting evidence in existing literature.

© 2015 Elsevier B.V. All rights reserved.

1. Introduction

It is known that organic materials degrade easily when light, moisture and/or oxygen are present simultaneously [1–5]; this is the reason for which organic electronic devices such as organic light emitting diodes (OLEDs) need to be encapsulated. Most of the studies regarding the device degradation are related to the operational degradation, i.e. film material is not studied alone but as an integral part of a working device [6,7]. Learning about degradation pathway of a single component and about its durability can help differentiate between various materials and unwanted processes that can occur during operation of a device.

Simultaneous presence of air and light may lead to degradation of organic thin films by interaction of the photo-excited molecules

with oxygen [4,8–13]. This interaction results in newly formed species – the impurities hereafter – which can significantly affect various film properties such as exciton diffusion length, luminescence, thermal (morphological) stability, etc. In favorable cases, like in anthracene–tetracene mixed crystals, the sensitized fluorescence measurements can detect impurity concentrations as low as one impurity molecule per ten billion host molecules [14]. This is possible because excited electronic states, i.e. the excitons in some molecular solids can diffuse during their radiative lifetime to reach quenching site at the distances which are comparable to the exciton diffusion length [15]. The understanding of the behavior under the influence of impurities may lead to technological progress that could extend the lifetime of organic electronic devices.

We study steady-state photoluminescence (PL) of amorphous films of 4,4′-bis(2,2-diphenylvinyl)-1,1′-biphenyl (DPVBi), an efficient blue emitter commonly used in the production of blue and white OLEDs (either in emissive or transporting layers) [16–19],

---

under influence of external conditions. Electroluminescent devices with blue emitters are particularly prompt to photodegradation in the presence of oxygen because of the high photon energy that can trigger photo-oxidation. Simultaneous exposure to UV light and oxygen introduces photo-oxidized molecules (the impurities) in the DPVBi films, leading to an efficient quenching of the steady-state PL with very low concentration of the impurities. This study offers a new insight into degradation mechanism of thin films of DPVBi, while other studies concerning this material [7,20] deal with operational degradation of OLEDs which contain thin film of DPVBi as a hole-transport layer.

Similar behavior of PL was previously noticed in our study of morphological stabilization of amorphous films by UV light of N,N′-bis(3-methylphenyl)-N,N′-bis(phenyl)benzidine (TPD), another well-known OLED material [21], and by other authors before us [22,23]. DPVBi and TPD have similar characteristics like molecular structure, UV–vis absorbance [24,25] and glass transition temperatures [26,27], but changes under UV light and oxygen are faster in DPVBi, what makes it easier to study.

In this work measurements of absorbance and PL of amorphous DPVBi films as function of time of exposure to UV light in vacuum, air and nitrogen and at different oxygen pressures were performed. Infrared and mass spectra of films before and after the exposure were also measured. Density functional theory (DFT) is applied to DPVBi and to some of its oxygenated derivative molecules and compared with measurements to get insight into the nature of induced impurities.

2. Experimental details

2.1. Sample preparation

Amorphous thin films of DPVBi (American Dye Source, 98% purity) were evaporated in high vacuum with 5×10^{-4} Pa of background pressure, using the Knudsen effusion cells with 3 mm pinhole. The temperature of evaporator was kept at 210 °C powered by Sorensen DCS8-125E and regulated by an active feedback loop. A typical deposition lasts for 15 min and produces films with thickness of about 200 nm. Film thickness d was determined from absorption measurements using the value of DPVBi absorption coefficient 1.07×10^5 cm^{-1} at 355 nm [25]. Films were deposited on substrates such as fused silica, a boron-silicate glass and KBr (Sigma Aldrich). Prior to deposition, substrates were cleaned with a detergent soap, sonicated in isopropanol and then in ultrapure water (Milli-Q 18.2 MΩ cm at 25 °C) and dried in a nitrogen flow. KBr substrate was used as received.

2.2. Irradiation

Films were exposed to UV light obtained from a 350 nm UV LED with maximum power density $I_{UV}^{max} = 3$ mW cm^{-2}, as measured by a Solar Light Co. PMA 2110 UVA sensor.

2.3. UV–vis spectroscopy

Changes in absorption spectrum of DPVBi films on fused silica substrates irradiated with $I_{UV} = 0.4$ mW cm^{-2} were measured by single beam Beckman Colter DU 700 spectrophotometer.

2.4. Photoluminescence and rate measurements

The same UV LED was used to excite PL spectra and to follow rates of change in PL and absorbance at 355 nm. In air PL spectra and the rates for absorbance at 355 nm were measured at the same spot on a film using Princeton Instruments Acton SP2500

spectrometer coupled with Pixis 100 CCD detector. In order to study rates of changes of absorbance and PL in different atmospheres (air, oxygen, nitrogen and vacuum), a setup was built which allowed measurements on the samples directly in the evaporation chamber.

2.5. Infrared spectroscopy

Infrared (IR) measurements were performed using Nicolet iN10 infrared microscope with a cooled detector, 300 μm × 300 μm sampling area, 256 scans and resolution of 4 cm^{-1} on pristine and irradiated (one hour of exposure to $I_{UV} = 1$ mW cm^{-2}) 400 nm thick DPVBi films deposited on KBr substrates.

2.6. Mass spectroscopy

Laser desorption ionization mass spectroscopy (LDI MS) was performed using the commercial matrix-assisted laser desorption and ionization time-of-flight Voyager Biospectrometry DE Pro Workstation (Perspective Biosystems, USA) on pristine and irradiated films deposited directly onto metallic sample holder (well plate) of the spectrometer. As DPVBi absorbs at the wavelength of the laser, matrix was not used. The pressure inside the workstation was kept at few 10^{-5} Pa so the laser, emitting at 337 nm, could not produce photo-oxidation of DPVBi films. The polarization was positive and laser intensity was 2000 with 330 shots. Another method of MS, using Waters Acquity Tandem Quadrupole Detector with atmospheric solids analysis probe (ASAP) set to detect positive ions, was performed to compare results with LDI MS. All data were obtained and processed using the MassLynx 4.1 software. ASAP technique enables ionization of non-polar compounds and is particularly convenient for our study as materials need not to be dissolved. Sample preparation is simple: material is scratched from the film with a clean capillary, which is immediately afterwards inserted in the chamber of the spectrometer. The polarization was positive, source temperature was at 150 °C, capillary temperature at 400 °C, corona and cone voltages were 3 keV and 20 V, respectively. Results form MLADI-TOF MS are in agreement with results from ASAP MS.

2.7. Theoretical calculations

We have carried out DFT modeling of molecular DPVBi and its possible photo-oxidation products with 0, 1 and 2 oxygen atoms attached, at B3LYP up to 6-311++G** level of theory using NWCHEM [28]. For each of them, we searched for the lowest-energy conformers (CFs, including the varying of the O-binding sites), considering in total about 300 geometries. The IR spectra were calculated for the lowest-energy CFs found and the obtained results compared with the experiment. For DPVBi molecule exactly four CFs were found with relative ground-state energies within only 1 kJ/mol. The absorption properties of the four CFs are barely distinguishable, since the frontier orbitals lie on the central two rings near attached carbons and are essentially not affected by the orientation of the outer rings by which the CF geometries differ.

3. Results and discussion

Photoluminescence intensity of DPVBi films exposed to UV light *in air* falls exponentially with time. Upon prolonged exposure, their UV–vis absorption spectra change, indicating a chemical alteration of film composition. Furthermore, when the partial pressure of oxygen is increased, these changes become faster. If, on the contrary, the films are exposed to UV light *in vacuum*, neither their PL nor absorbance would change with the time of exposure
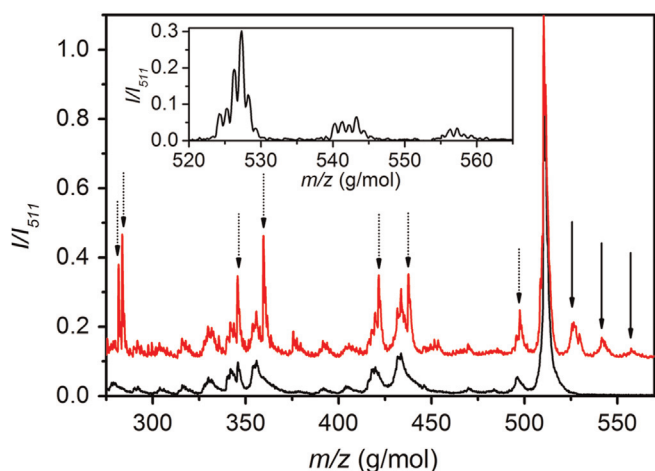
Fig. 1. LDI mass spectra, without any matrix, recorded in the positive ion mode, of pristine (bottom curve) and UV irradiated (top curve) films normalized to their intensity I_{511} at $M_{DPVBi}=511$ g/mol, the mass of DPVBi and offset by 0.1 for clarity. The inset shows the group of masses $M > M_{DPVBi}$ obtained by ASAP MS of UV irradiated film.

Fig. 2. IR spectra of DPVBi pristine film (bottom curve) and film irradiated for one hour with $I_{UV}=1$ mW cm^{-2} (top curve). Spectra are offset 1 a.u. for clarity.

(on the timescale and under UV illumination conditions of experiments presented here). Thus, the simultaneous presence of UV light and oxygen is needed for the degradation of DPVBi films.

3.1. Photo-oxidation of DPVBi films

In order to investigate photo-chemical changes of DPVBi film composition upon its simultaneous exposure to UV light and air, a comparison of mass spectra of pristine and exposed films was performed (Fig. 1). Mass spectra of DPVBi pristine thin films show dominant peak at $M_{DPVBi}=510.6$ g/mol, which corresponds to the mass of DPVBi molecule. Besides this, other smaller masses can be observed, which are attributed to fragments of DPVBi induced by MS technique. Irradiated samples show the presence of numerous new species – impurities (indicated by arrows), which can be divided into two groups. One group, with $M > M_{DPVBi}$ (solid arrows), is presumed to consist of oxygenated DPVBi molecules. These masses seem to follow a pattern: $M_{x,y,z}=M_{DPVBi}+x\Delta M_1+y\Delta M_2+z\Delta M_3$, where $M_{x,y,z}$ is the mass of new species and x, y and z may take integer values 0, 1, 2 or 3 (inset of Fig. 1). Masses $\Delta M_1=14$ g/mol, $\Delta M_2=15$ g/mol and $\Delta M_3=16$ g/mol correspond to the molecule gaining one oxygen atom and losing two, one or zero hydrogen atoms, respectively. The loss of two H atoms implies that O atom formed a bridge between two C atoms. If one H atom is lost, then it is expected that O forms a double bond with C and, finally, if no H atom is lost, it is plausible that –OH group is attached to C atom. The other group, with $M < M_{DPVBi}$ (dotted arrows), is supposed to consist of molecular fragments of oxygenated DPVBi (fragments of impurities with $M > M_{DPVBi}$, induced by MS technique) and/or of photo-oxidation products. Results of MS suggest that the photo-oxidation of DPVBi happens when films are exposed to air and UV light.

The presence of dimers of DPVBi was not detected in irradiated samples. Relative intensity of peaks in mass spectra does not necessarily reflect relative number of different molecules present in a film, as different species do not necessarily have the same ionization cross section. Thus, it is not possible to deduce which type of impurity is predominant.

Further evidence for photo-oxidation is provided by infrared spectroscopy. The measured IR spectra of pristine and irradiated DPVBi film are shown in Fig. 2. In the case of the irradiated sample new broad features can be observed in the regions around 1250,
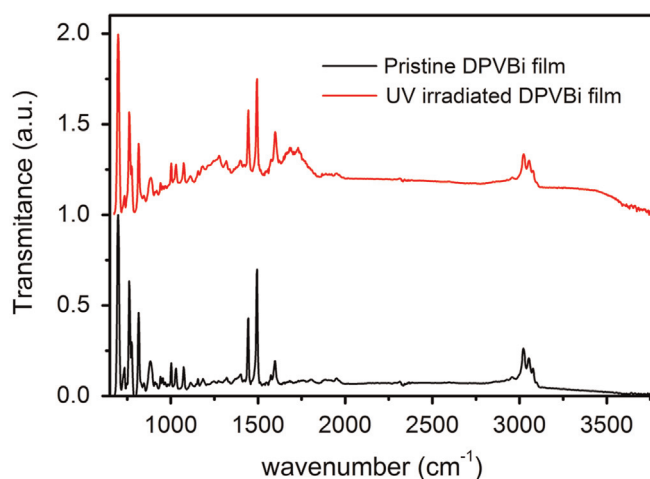
1700 and 3300 cm^{-1}. The new features have large width as a consequence of a superposition of a large number of characteristic vibrational frequencies with slightly different eigenvalues and by inhomogeneous broadening in the amorphous medium of DPVBi film. IR spectra are in agreement with results obtained from MS: we assume that the feature around 1700 cm^{-1} belongs to C=O bond (ΔM_2), while the one around 1250 cm^{-1} can be ascribed to C–O bond (ΔM_1, if O bound to two C atoms or ΔM_3). Broad feature around 3300 cm^{-1} could be explained by the presence of –OH groups (ΔM_3), possibly participating in hydrogen bonding [29]. While MS shows the presence of new masses which correspond to formation of hydroxyl groups, IR spectra do not show pronounced –OH peak.

To give support to conclusions drawn in the previous paragraph, theoretical DFT molecular vibrational spectra were calculated for some possible photo-induced impurities. Comparison of the pristine DPVBi IR spectrum with the DFT result, given in Fig. 3a, shows that theoretical molecular spectra can well describe the experimental ones. The lower band properties (600–1600 cm^{-1}) are in a good agreement with the experiment. The upper band (~ 3000 cm^{-1}) shows a red-shift relative to the measured spectra, but it is difficult to discern whether the difference is a systematic error of DFT or a genuine difference between the molecular and thin film DPVBi spectra.

In Fig. 3b experimental IR spectrum of illuminated film is compared with DFT molecular spectra of oxidized DPVBi, calculated at B3LYP/6-311++G** level, for the lowest energy CFs found. There are three important conclusions to be drawn from the comparison: (a) numerous lines found by DFT fall in the region of 1250 cm^{-1} feature, many of them belonging to C–O bond, while only few of them belong to pure DPVBi molecule; (b) the feature about 1700 cm^{-1} consists of two nearby broad peaks and DFT results suggest that these cannot belong to a molecular pristine DPVBi since there are no vibrations in its spectra between 1600 cm^{-1} and 2900 cm^{-1} (see Fig. 3a). In contradistinction, molecule with two O attached to a phenyl ring has an in-plane stretching of the C=O vibration at 1690 cm^{-1} (denoted $M1_{0,2,0}$ in Fig. 3b). The lowest energy $M_{0,2,0}$ found has an in-plane oscillation of the C=O bond at 1730 cm^{-1}, in a very good agreement with the frequency of the second peak of the feature (both calculated at B3LYP/6-311++G** level); and, (c) DFT results for IR spectra of the molecular DPVBi with one or two hydroxyl groups ($M_{0,0,1}$ and $M_{0,0,2}$) give strong peaks around 3590 cm^{-1} corresponding to an –OH stretching mode. Since there are no strong peaks above 3100 cm^{-1} in the measurement, we conclude that the noncovalent
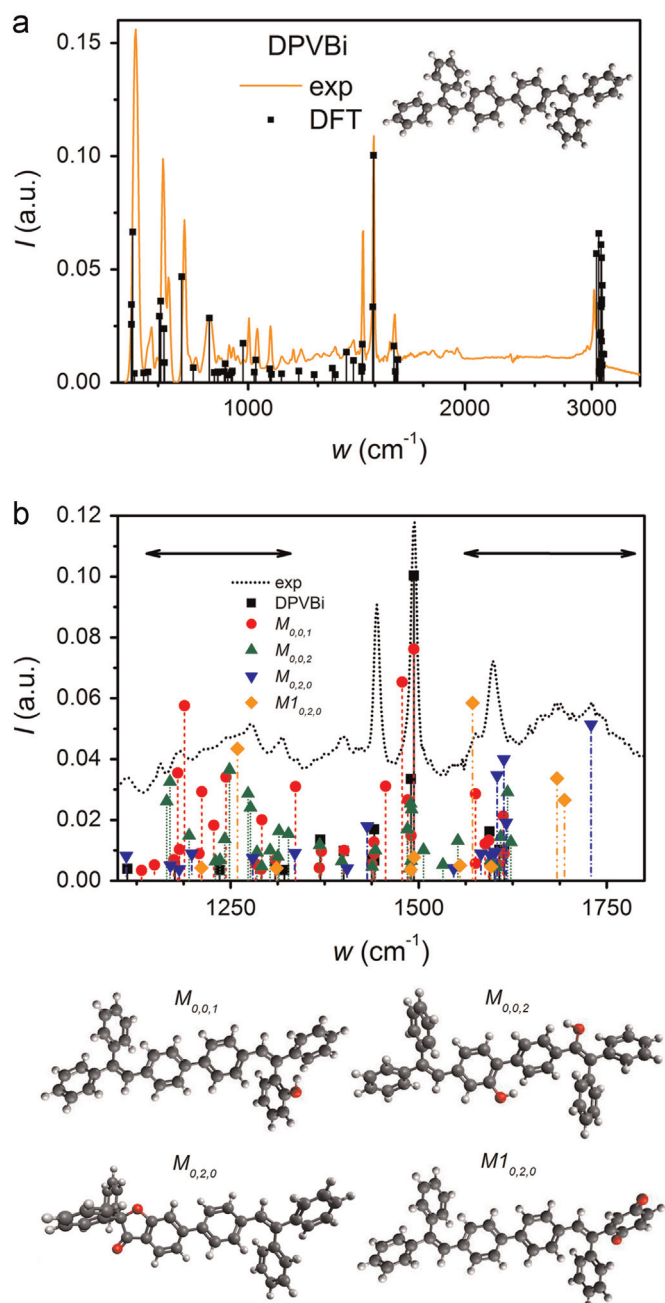
Fig. 3. (a) Comparison of experimentally measured IR spectrum of unexposed DPVBi film (continuous line) and the molecular DPVBi IR spectrum calculated at B3LYP/6-311++G** level (dots and vertical lines) in semi-log plot. In the inset is the image of DPVBi molecule. (b) Comparison of experimentally measured IR spectrum of exposed DPVBi film (dotted line) and the molecular IR spectra (vertical lines) calculated at B3LYP/6-311++G** level for DPVBi (squares) and several possible photo-oxidation products (their structure is given in the lower panel) denoted by $M_{0,0,1}$ (circles), $M_{0,0,2}$ (upward triangles), $M_{0,2,0}$ (downward triangles) and $M1_{0,2,0}$ (diamonds). Oxygen atoms are indicated as red. Arrows indicate the regions of broad features around 1250 and 1700 cm^{-1}, which appear only in exposed films (see Fig. 2). Intensities (y-axis) in both (a) and (b) are in arbitrary units, while x-axis shows the wavenumber in cm^{-1}. (For interpretation of the references to color in this figure legend, the reader is referred to the web version of this article.)

interactions between new species and surrounding molecules strongly damp and broaden vibrations of –OH group.

From the MS and IR spectra one sees that new species are photo-oxidized DPVBi molecules or its fragments with one, two
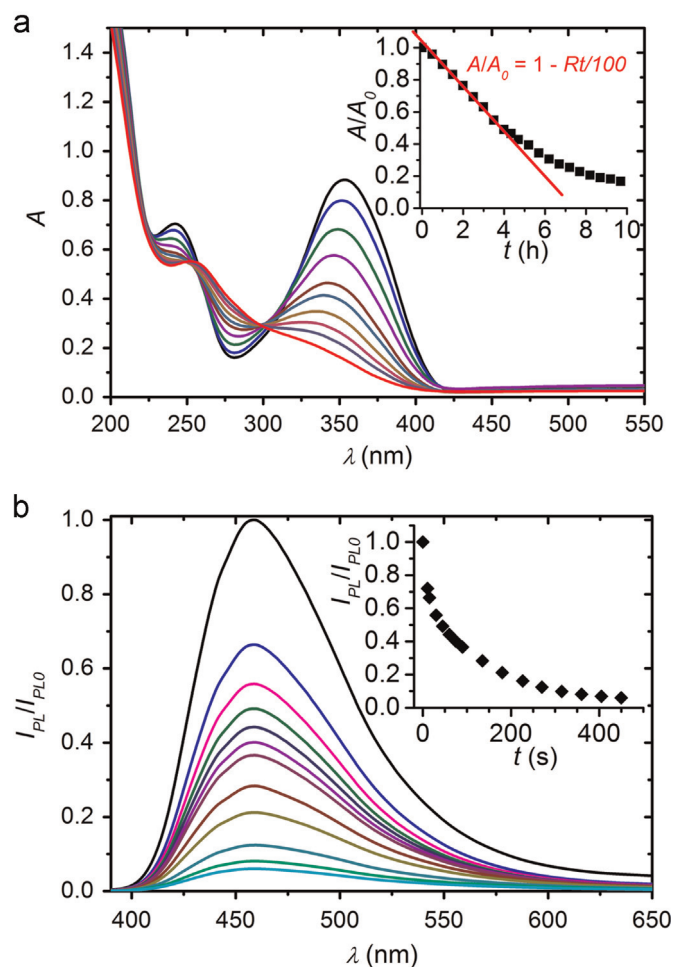

Fig. 4. (a) Absorbance A vs. λ as a function of irradiation time $t=0$, 1, 2, 3, 4, 4.7, 5.7, 6.7, 7.7 and 9.7 h, where A decreases monotonically with t. Inset in (a) shows plot of absorbance A at $\lambda=355$ nm normalized to its initial value A_0 as a function of t and linear fit that defines the rate R of change of absorbance. (b) Photoluminescence I_{PL}, normalized to the value I_{PL0} at $\lambda=458$ nm and $t=0$ s, vs. λ plotted for $t=0$, 15, 30, 45, 60, 75, 90, 135, 180, 270, 360 and 450 s, where I_{PL}/I_{PL0} decreases monotonically with t. Inset of (b) shows I_{PL}/I_{PL0} at 458 nm normalized to its initial value as function of t. In both measurements 190 nm thick DPVBi films were irradiated in air with $I_{UV}=0.4$ mW cm^{-2}.

and even three oxygen atoms added, which can be singly or doubly bound to C atoms of DPVBi.

Fig. 4a shows absorption spectra as a function of wavelength λ after different times of *irradiation in air* of 190 nm thick DPVBi film deposited onto fused silica substrate and irradiated with $I_{UV}=0.4$ mW cm^{-2}. Pristine film (no irradiation) shows two absorption bands at 242 and 355 nm, corresponding to two lowest excited electronic states. The energy gap is (3.0 ± 0.1) eV, estimated from the long-wavelength absorption edge [30], in a good agreement with our TD-B3LYP/6-311++G** result for the first excitation of DPVBi in the lowest vibrational state being at 3.14 eV. Irradiation with UV light induces gradual disappearance of both bands and emergence of new peak around 255 nm, reflecting a gradual chemical change in film composition (degradation of DPVBi) and a formation of photo-oxidized products of DPVBi. The percent of change in the value of absorbance A at $\lambda=355$ nm is assumed to be roughly the same as the percent of impurities present in a film. To track this change, A taken at 355 nm, normalized to its initial value A_0 at time $t=0$, is plotted in the inset of Fig. 4a as a function of irradiation time t. The decrease in normalized absorbance A/A_0 is close to linear at the beginning and then gradually slows down. Nonlinear part of the curve can be a
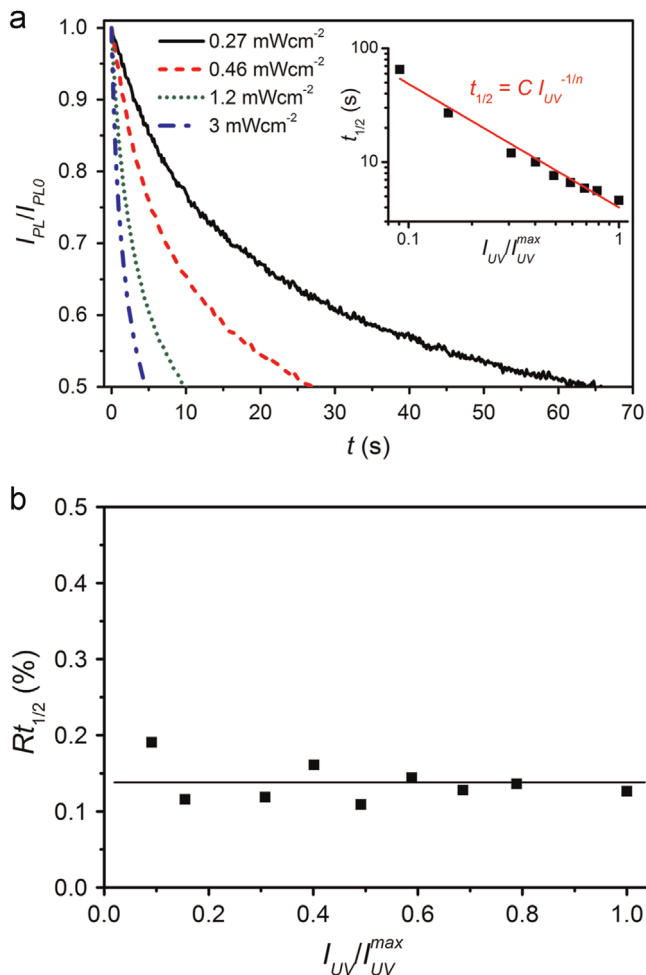
Fig. 5. (a) Photoluminescence I_{PL}/I_{PL0} at 458 nm vs. t of 190 nm thick DPVBi films obtained for different intensities of UV light. Inset shows $t_{1/2}$ as a function of I_{UV}/I_{UV}^{max} and a fit $t_{1/2}=CI_{UV}^{-1/n}$ that gives $n=(1.08\pm0.06)$. (b) The product of $Rt_{1/2}$ as a function of normalized UV light intensity I_{UV}/I_{UV}^{max}.

Fig. 6. (a) Photoluminescence I_{PL}/I_{PL0} at 458 nm and (b) absorbance A/A_0 at 355 nm vs. t of 190 nm thick DPVBi films irradiated with I_{UV}^{max} recorded in vacuum (10^{-4} Pa, open downward triangles), nitrogen at 100 kPa (open upward triangles), different oxygen pressures (solid symbols) and air at 100 kPa (solid stars). In (a) top x-axis (in minutes) refers to measurements in vacuum and nitrogen (open symbols and indicated by arrow), while bottom x-axis (in seconds) refers to measurements in different oxygen pressures and air. Curves obtained in air and at oxygen pressure of 24 kPa have similar rates due to the fact that the partial pressure of oxygen in air is around 20 kPa.

consequence of change in degradation process dynamics due to a significant loss of DPVBi material (around 60%). From the linear part the rate R of change of normalized absorbance A/A_0 is defined by $A/A_0=1-Rt/100$ (the inset of Fig. 4a and for the film from Fig. 4 it is around 0.22%/min.

Effects which degradation *in air* has on the photoluminescence (PL) are shown in Fig. 4b as a series of spectra of a 190 nm thick film irradiated with UV intensity $I_{UV}=0.4$ mW cm^{-2} as function of irradiation time t. Irradiation induces no new bands in PL spectrum. Inset in Fig. 4b shows that PL intensity I_{PL} at $\lambda=458$ nm, normalized to its value I_{PL0} at $t=0$, has a quick, exponential decay with t. Time necessary for PL intensity to drop to half of its initial value – half lifetime $t_{1/2}$ is 45 s. During that time, according to the value of R, absorbance changed only for a little less than 0.2%, pointing to some non-trivial mechanism of PL quenching.

The influence of different UV light intensities on the sample degradation *in air* was also studied: the rate R and time evolution of I_{PL}/I_{PL0} at 458 nm were measured as function of I_{UV} for 190 nm thick film. Photoluminescence I_{PL} has exponential decay which is faster for larger I_{UV} (Fig. 3a), while the rate R is proportional to I_{UV}. In the inset of Fig. 3a, $t_{1/2}$ was plotted versus I_{UV}/I_{UV}^{max}, along with the fit to the relation $t_{1/2}=CI_{UV}^{-1/n}$ used for OLEDs [7]; C is a constant and n is so-called acceleration parameter, whose value is (1.08 ± 0.06). This means that $t_{1/2}$ is, to a good approximation, inversely proportional to I_{UV}. The product of R and $t_{1/2}$, which is the percentage of changed absorbance or DPVBi molecules that
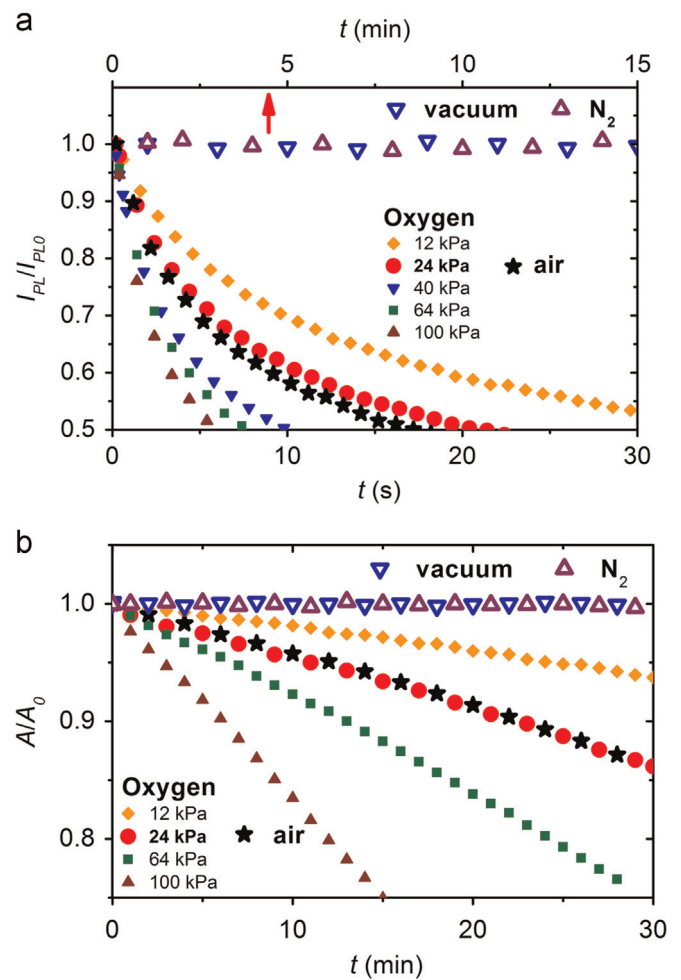
leads to 50% decay of PL, should be then approximately independent of I_{UV}, as $R\sim I_{UV}$. This is shown in Fig. 3b where the product $Rt_{1/2}$ stays approximately constant and less than 0.2% when I_{UV} varies. Eventual dependence of $Rt_{1/2}$ on I_{UV} would indicate that dynamics of formation of impurities is not the same for different UV light intensities Fig. 5.

Photoluminescence spectra of DPVBi films in high vacuum (5×10^{-4} Pa) and nitrogen atmosphere (Fig. 6a) show no change even for irradiation times of 15 min with I_{UV}^{max}. Under the same conditions, the rate R of change of absorbance is zero (Fig. 6b). Thus, under the conditions and on the time scale of our experiments, no change in film composition can be induced by UV light *in vacuum*. Likewise, PL does not change when films are exposed only to air: PL of DPVBi film was first measured in situ in vacuum (briefly exposed *only to UV light*), then the film was exposed *only to air* (no UV light) so that oxygen enters the film [12,13] and, finally, brought back to low vacuum (few Pa), where PL was recorded once again (the two measured values of PL were the same). An implication, for practical purposes, would be that even the low vacuum is sufficient for extraction of oxygen from amorphous DPVBi films of thickness of order of 200 nm. Additionally, both rates of change
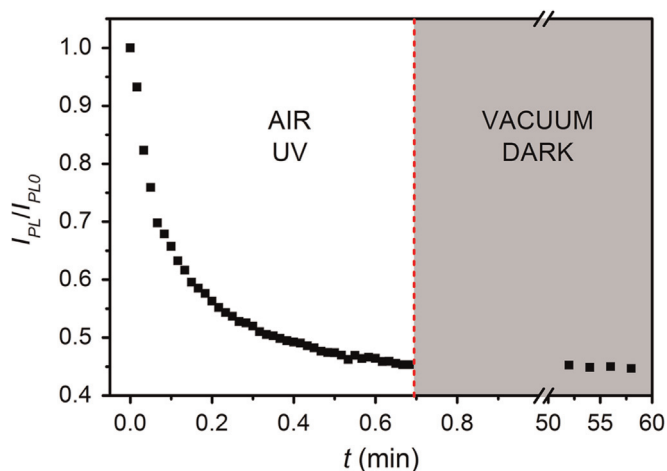
Fig. 7. Normalized PL intensity I_{PL}/I_{PL0} at 458 nm vs. t of a film exposed to $I_{UV} = 0.45$ mW cm^{-2} *in air* followed by a quick evacuation of air to a few Pa. Then the measurement was paused and film kept in vacuum with UV light off. After 50 min few PL measurements were taken in given conditions.

of absorbance and PL increase with the increase of oxygen pressure as shown in Fig. 6. These considerations imply that the *simultaneous* presence of oxygen and UV light is necessary for degradation of DPVBi films and that the *excited DPVBi molecules interact with oxygen* to produce impurities.

In general, there are two possible pathways for chemical reaction of DPVBi and oxygen, both typical for such compounds [8,31]. In one of them excited singlet molecule gives an electron to ground-state oxygen molecule to form radical cation and the superoxide anion, which can further react chemically to form new species [31]. In the other, host molecule in excited triplet state acts as a sensitizer and transfers its energy to ground-state triplet oxygen to form singlet oxygen and ground-state host molecule [31]. The energy needed for singlet oxygen formation is 0.97 eV. The first excited triplet state of DPVBi, according to our TD-B3LYP/6-311++G** calculation, is 2.19 eV, which is in a good agreement with experimental value of 2 eV obtained for spiro-DPVBi [32]. This energy is sufficient for singlet oxygen formation in our films. Singlet oxygen is very reactive and may further interact with other DPVBi molecules to form photo-oxidized species. We find by DFT that DPVBi can form a bound state with singlet oxygen, with the binding energy of 0.17 eV, but could not find any bound state in the triplet case.

3.2. The mechanism of photoluminescence quenching by induced impurities

Oxygen is a well-known PL quencher [12,13]. However, we find no evidence for direct collisional quenching with oxygen. If this type of quenching was present, PL intensity would be (partially) reversible after removal of oxygen from the film. In the following experiment it was demonstrated that PL is not reversible (Fig. 7): first a film was UV-degraded *in air* for about $t_{1/2}$, then the air was evacuated to the pressure of few Pa in a few seconds and the film kept in vacuum for 50 min in dark. After 50 min several measurements of PL were carried out, which show that its value remained the same as the one at the end of the degradation in air. Thus, PL quenching is only due to new photo-oxidized species.

At the level of 0.2% of impurities (that quench 50% of PL), the average distance between impurity molecules d_i is around 7 nm. This value is obtained taking the density of DPVBi to be 1.2 g cm^{-3} (that of monoclinic crystal with two molecules per unit cell) [33] and assuming that molecules form a simple cubic lattice. The long-

range Förster resonant energy transfer (FRET) from DPVBi to impurity molecule can be ruled out due to absence of a spectral overlap between DPVBi emission centered at 458 nm and the impurity absorption at 255 nm [15,34–36]. Thus, only reasonable assumption on the mechanism of PL quenching is that the excitons diffuse through the film at long distance and, if during their lifetime an impurity molecule is reached, quenching as the most probable outcome may happen [15,37–41]. Exciton diffusion length l_D for amorphous DPVBi films is measured by Choukri [42] to be (8.7 ± 0.6) nm and satisfies the condition $d_i < l_D$ required for quenching [43].

The Förster energy transfer among DPVBi molecules occurs with the probability higher than 50% when their separation is smaller than 1.4 nm. The Förster self-radius $R_0 = 1.4$ nm for DPVBi is calculated from the formula $R_0 = 0.211(\kappa^2 n^{-4} Q_D J(\lambda))^{1/6}$ [44], where $\kappa^2 = 2/3$ is the geometrical factor for random orientation of the donor and acceptor transition dipole moments, $Q_D = 0.45$ is PL quantum efficiency of amorphous DPVBi [45] and $J(\lambda) = 4 \times 10^{12}$ (nm)^4 M^{-1} cm^{-1} is the overlap integral between PL and absorption spectra of DPVBi. As, to the best of our knowledge, experimental data for the refractive index n of DPVBi are lacking, we have, instead, taken the value $n = 2$ of structurally similar TPD molecule [46]. Excitations are localized and move by hopping from one DPVBi molecule to another via one of two possible processes: one is FRET and the other is Dexter electron transfer [47]. Dexter's mechanism requires a spatial overlap between wave functions of DPVBi molecules and it occurs only at short distances, typically not larger than 1 nm. The rate of Dexter transfer is typically much lower than the rate of FRET, as it applies to excitons with dipole-forbidden transitions, like in triplet–triplet energy transfers [15,39]; in the case of DPVBi, PL is due to singlet excitons, thus, hopping would likely occur through FRET.

Oxygen diffuses into amorphous film, where it reacts with excited DPVBi molecule and forms an impurity, which acts as quenching site. Exciton diffuses by hopping form one DPVBi to another through FRET in a random walk manner. If, during its lifetime, it comes to proximity of an impurity, a Dexter-type energy transfer occurs and PL is quenched.

4. Conclusion

Thin DPVBi films were irradiated by UV light in ambient, vacuum and under different oxygen pressures. Films of DPVBi are degraded by UV light only in the presence of oxygen. The degradation is a consequence of reaction between *UV-excited* DPVBi molecules and oxygen. Films of DPVBi can be safely removed from vacuum as long as there is no interaction with UV light and be returned to vacuum for further processing without change in composition. Reaction rates increase by increasing oxygen concentration and/or UV light intensity. Mass spectroscopy showed the presence of numerous new species generated by photo-oxidation of original compound. Also, the IR spectroscopy supports this finding.

Time needed for absorbance to drop to half of its value is two orders of magnitude larger than equivalent time for PL. For the most intense UV irradiation that was used, this time for PL is about 5 s and during that time absorbance drops only for a few tenths of percent. There is a non-trivial quenching mechanism of PL: it is a consequence of exciton diffusion from excited DPVBi to impurity molecule, assuming that excitons move via Förster resonant energy transfer by hopping. Thus, only a small fraction of percent of photo-oxidized species is sufficient to quench the luminescence in amorphous DPVBi films.

As DPVBi is used as emissive layer in OLEDs, findings of this work are important because they show that even a small amount

of oxygen that penetrates a DPVBi layer would impair luminescence efficiency of a device. Moreover, the absorption of its own radiation (around 400 nm) would additionally contribute to the rate of degradation of a device. It is reasonable to expect that the transport properties would also be affected in DPVBi based OLEDs.

Acknowledgment

References

[1] H. Neugebauer, C. Brabec, J.C. Hummelen, N.S. Sariciftci, Stability and photo-degradation mechanisms of conjugated polymer/fullerene plastic solar cells, Sol. Energy Mater. Sol. Cells 61 (2000) 35–42.

[2] K. Kawano, R. Pacios, D. Poplavskyy, J. Nelson, D.D.C. Bradley, J.R. Durrant, Degradation of organic solar cells due to air exposure, Sol. Energy Mater. Sol. Cells 90 (2006) 3520–3530.

[3] R. Pacios, A.J. Chatten, K. Kawano, J.R. Durrant, D.D.C. Bradley, J. Nelson, Effects of photo-oxidation on the performance of poly[2-methoxy-5-(3′,7′-dimethyloctyloxy)-1,4-phenylene vinylene]:[6,6]-phenyl C_{61}-butyric acid methyl ester solar cells, Adv. Funct. Mater. 16 (2006) 2117–2126.

[4] S. Cook, A. Furube, R. Katoh, Matter of minutes degradation of poly(3-hexylthiophene) under illumination in air, J. Mater. Chem. 22 (2012) 4282–4289.

[5] S. Schmidbauer, A. Hohenleutner, B. König, Studies on the photodegradation of red, green and blue phosphorescent OLED emitters, Beilstein J. Org. Chem. 9 (2013) 2088–2096.

[6] F. So, D. Kondakov, Degradation mechanisms in small-molecule and polymer organic light-emitting diodes, Adv. Mater. 22 (2010) 3762–3777.

[7] R. Siefert, S. Scholz, B. Lüssem, K. Leo, Comparison of ultraviolet- and charge-induced degradation phenomena in blue fluorescent organic light emitting diodes, Appl. Phys. Lett. 97 (2010) 013308.

[8] A. Maliakal, K. Raghavachari, H. Katz, E. Chandross, T. Siegrist, Photochemical stability of pentacene and a substituted pentacene in solution and in thin films, Chem. Mater. 16 (2004) 4980–4986.

[9] A.B. Djurišić, T.W. Lau, C.Y. Kwong, L.S.M. Lam, W.K. Chan, Evolution of optical properties of tris (8-hydroxyquinoline) aluminum (Alq_3) with atmosphere exposure, Proc. SPIE 4800 (2003) 200–207.

[10] V.K. Shukla, S. Kumar, D. Deva, Light induced effects on the morphology and optical properties of tris-(8-hydroxyquinoline) aluminium (Alq_3) small molecular thin film, Synth. Met. 156 (2006) 387–391.

[11] T. Zyung, J.-J. Kim, Photodegradation of poly(p-phenylenevinylene) by laser light at the peak wavelength of electroluminescence, Appl. Phys. Lett. 67 (1995) 3420–3422.

[12] H. Hintz, H.-J. Egelhaaf, L. Lüer, J. Hauch, H. Peisert, T. Chassé, Photodegradation of P3HT – a systematic study of environmental factors, Chem. Mater. 23 (2011) 145–154.

[13] L. Lüer, H.-J. Egelhaaf, D. Oelkrug, G. Cerullo, G. Lanzani, B.-H. Huisman, D. de Leeuw, Oxygen-induced quenching of photoexcited states in polythiophene films, Org. Electron. 5 (2004) 83–89.

[14] Von K.W. Benz, H.C. Wolf, Die konzentrationsabhängigkeit der energie-übertragung in anthracen-tetracen-mischkristallen, Z. Naturforschg. 19a (1964) 177–181.

[15] M. Pope, C.E. Swenberg, Electronic Processes in Organic Crystals and Polymers, second ed., Oxford University Press, New York, 1999.

[16] X. Zhang, Z. Wu, B. Jiao, D. Wang, D. Wang, X. Hou, W. Huang, Solution-processed white organic light-emitting diodes with mixed-host structures, J. Lumin. 132 (2012) 697–701.

[17] G. Li, J. Shinar, Combinatorial fabrication and studies of bright white organic light-emitting devices based on emission from rubrene-doped 4,4′-bis(2,2′-diphenylvinyl)-1,1′-biphenyl, Appl. Phys. Lett. 83 (2003) 5359–5361.

[18] S.E. Shaheen, G.E. Jabbour, M.M. Morrell, Y. Kawabe, B. Kippelen, N. Peyghambarian, M.F. Nabor, R. Schlaf, E.A. Mash, N.R. Armstrong, Bright blue organic light-emitting diode with improved color purity using a LiF/Al cathode, J. Appl. Phys. 84 (1998) 2324–2327.

[19] C. Hosokawa, H. Higashi, H. Nakamura, T. Kusumoto, Highly efficient blue electroluminescence from a distyrylarylene emitting layer with a new dopant, Appl. Phys. Lett. 67 (1995) 3853–3855.

[20] S. Winter, S. Reineke, K. Walzer, K. Leo, Photoluminescence degradation of blue OLED emitters, Proc. SPIE 6999 (2008) 69992N.

[21] A.Ž. Tomović, N. Markešević, M. Scarpellini, S. Bovio, E. Lucenti, P. Milani, R. Zikic, V.P. Jovanović, V.I. Srdanov, Stabilization of N,N′-bis(3-methylphenyl)-N,N′-bis(phenyl)benzidine thin film morphology with UV light, Thin Solid Films 562 (2014) 99–103.

[22] E.M. Han, J.J. Yun, G.C. Oh, S.M. Park, N.K. Park, Y.S. Yoon, M. Fujihira, Enhanced stability of organic thin films for electroluminescence by photoirradiation, Opt. Mater. 21 (2002) 243.

[23] Y. Qiu, J. Qiao, Photostability and morphological stability of hole transporting materials used in organic electroluminescence, Thin Solid Films 372 (2000) 265.

[24] H. Mattoussi, H. Murata, C.D. Merritt, Y. Iizumi, J. Kido, Z.H. Kafafi, Photoluminescence quantum yield of pure and molecularly doped organic solid films, J. App. Phys. 86 (1999) 2642.

[25] T. Fukuda, B. Wei, M. Ichikawa, Y. Taniguchi, Transient characteristics of organic light-emitting diodes with efficient energy transfer in emitting material, Thin Solid Films 518 (2009) 567–570.

[26] K. Naito, A. Miura, Molecular design for nonpolymeric organic dye glasses with thermal stability: relations between thermodynamic parameters and amorphous properties, J. Phys. Chem. 97 (1993) 6240.

[27] S. Wang, W.J. Oldham Jr., R.A. Hudack Jr., G.C. Bazan, Synthesis, morphology, and optical properties of tetrahedral oligo(phenylenevinylene) materials, J. Am. Chem. Soc. 122 (2000) 5695–5709.

[28] M. Valiev, E.J. Bylaska, N. Govind, K. Kowalski, T.P. Straatsma, H.J.J. van Dam, D. Wang, J. Nieplocha, E. Apra, T.L. Windus, W.A. de Jong, NWChem: a comprehensive and scalable open-source solution for large scale molecular simulations, Comput. Phys. Commun. 181 (2010) 1477.

[29] J. Workman Jr., The Handbook of Organic Compounds, Academic Press, San Diego, 2000.

[30] P.E. Burrows, Z. Shen, V. Bulovic, D.M. McCarty, S.R. Forrest, J.A. Cronin, M. E. Thompson, Relationship between electroluminescence and current transport in organic heterojunction light-emitting devices, J. Appl. Phys. 79 (1996) 7991–8006.

[31] G.J. Kavarnos, Fundamentals of Photoinduced Electron Transfer, VCH Publishers, New York, 1993.

[32] G. Schwartz, Novel Concepts for High-efficiency White Organic Light-emitting Diodes, Technischen Universität Dresden, Dresden, 2007 (PhD thesis).

[33] H.-N. Liu, G. Zhang, L. Hu, P.-F. Su, Y.-F. Li, 4,4′-Bis(2,2-diphenylvinyl)-1,1′-biphenyl, Acta Crystallogr. E67 (2011) o220.

[34] Th Förster, 10th Spiers memorial lecture. Transfer mechanisms of electronic excitation, Discuss. Faraday Soc. 27 (1959) 7–17.

[35] T. Virgili, D.G. Lidzey, D.D.C. Bradley, Efficient energy transfer from blue to red in tetraphenylporphyrin-doped poly(9,9-dioctylfluorene) light-emitting diodes, Adv. Mater. 12 (2000) 58–62.

[36] E. Suljovrujic, A. Ignjatovic, V.I. Srdanov, T. Mitsumori, F. Wudl, Intermolecular energy transfer involving an iridium complex studied by a combinatorial method, J. Chem. Phys. 121 (2004) 3745–3750.

[37] W. Klöpffer, Transfer of electronic excitation energy in polyvinyl carbazole, J. Chem. Phys. 50 (1969) 2337–2343.

[38] D.C. Northrop, O. Simpson, Electronic properties of aromatic hydrocarbons. II Fluorescence transfer in solid solutions, Proc. R. Soc. Lond. A 234 (1956) 136–149.

[39] C. Madigan, V. Bulović, Modeling of exciton diffusion in amorphous organic thin films, Phys. Rev. Lett. 96 (2006) 046404.

[40] T.-S. Ahn, N. Wright, C.J. Bardeen, The effects of orientational and energetic disorder on Forster energy migration along a one-dimensional lattice, Chem. Phys. Lett. 446 (2007) 43–48.

[41] S.M. Menke, R.J. Holmes, Exciton diffusion in organic photovoltaic cells, Energy Environ. Sci. 7 (2014) 499–512.

[42] H. Choukri, A. Fischer, S. Forget, S. Chénais, M.-C. Castex, D. Adès, A. Siove, B. Geffroy, White organic light-emitting diodes with fine chromaticity tuning via ultrathin layer position shifting, Appl. Phys. Lett. 89 (2006) 183513.

[43] O.V. Mikhnenko, M. Kuik, J. Lin, N. van der Kaap, T.-Q. Nguyen, P.W.M. Blom, Trap-limited exciton diffusion in organic semiconductors, Adv. Mater. 26 (2014) 1912–1917.

[44] J.R. Lakowicz, Principles of Fluorescence Spectroscopy, third ed., Springer Science+Business Media, New York, 2006.

[45] K.O. Cheon, J. Shinar, Förster energy transfer in combinatorial arrays of selective doped organic light-emitting devices, Appl. Phys. Lett. 84 (2004) 1201–1203.

[46] W. Holzer, A. Penzkofer, H.-H. Horhold, Travelling-wave lasing of TPD solutions and neat films, Synth. Met. 113 (2000) 281.

[47] D.L. Dexter, A theory of sensitized luminescence in solids, J. Chem. Phys. 21 (1953) 836–850.

Designing topological defects in 2D materials using scanning probe microscopy and a self-healing mechanism: a density functional-based molecular dynamics study

Designing topological defects in 2D materials using scanning probe microscopy and a self-healing mechanism: a density functional-based molecular dynamics study

Igor Popov,[1, 2] Ivana Djurišić,[2] and Milivoj Belić[3]

[1]*Institute for Multidisciplinary Research, University of Belgrade, Kneza Višeslava 1a, 11000 Belgrade, Serbia*
[2]*Institute of Physics Belgrade, University of Belgrade, Pregrevica 118, 11000 Belgrade, Serbia**
[3]*Science Program, Texas A & M University at Qatar, P.O. Box 23874, Qatar*

Engineering of materials at the atomic level is one of the most important aims of nanotechnology. The unprecedented ability of scanning probe microscopy to address individual atoms opened the possibilities for nanomanipulation and nanolitography of surfaces and later on of two-dimensional materials. While the state-of-the-art scanning probe lithographic methods include primarily adsorption, desorption and repositioning of adatoms and molecules on substrates or tailoring nanoribbons by etching of trenches, the precise modification of the intrinsic atomic structure of materials is yet to be advanced. Here we introduce a new concept, scanning probe microscopy with a rotating tip, for engineering of atomic structure of membranes based on two-dimensional materials. In order to indicate the viability of the concept, we present our theoretical research, which includes atomistic modelling, molecular dynamics simulations, Fourier analysis and electronic transport calculations. While stretching can be employed for fabrication of atomic chains only, our comprehensive molecular dynamics simulations indicate that the nanomanipulation by scanning probe microscope with a rotating tip is capable of assembling a wide range of topological defects in two-dimensional materials in a rather controllable and reproducible manner. We analyze two possibilities. In the first case the probe tip is retracted from membrane while in the second case tip is released beneath membrane allowing graphene to freely relax and self-heal the pore made by tip. The former approach with the tip rotation can be achieved experimentally by rotation of sample which is equivalent to rotation of the tip, whereas irradiation of membrane by nanoclusters can be utilized for the latter approach. The latter one has a potential to yield yet a richer diversity of topological defects on account of a lesser determinacy. If successfully realized experimentally the concept proposed here can be an important step toward a controllable nanostructuring of two-dimensional materials.

INTRODUCTION

Precise, accurate and predictable nanostructuring is an ultimate goal of nanophysics and nanotechnology. Scanning probe microscopy (SPM) including scanning tunneling microscopy (STM) [1] and atomic force microscopy (AFM)[2] have proven records of their capabilities for nanostructuring (i.e. scanning probe nanostructuring - SPN) at the nanometer level. An impressive precision was demonstrated already in 1989 by Don Eigler who manipulated 35 individual Xenon atoms on a nickel substrate [3]. The first nanostructuring demonstration was followed by nanoscale patterning of H-passivated Si(100) surface by STM [4], which paved a way for using STM as a tool in lithography processes [5]. The focus of research in SPN techniques has been mainly on adsorption, desorption and manipulation of adatomic and molecular decorations of substrates [6–11]. The local anodic oxidation (LAO)[12, 13] is also often utilized, which can provide a spatially-controlled modification of various materials including graphene sheets [14]. Complex structures with lithographic resolutions down to 25 nm have been demonstrated using the AFM method [15, 16], whereas much higher spatial resolutions down to 2.5 nm have been achieved by STM in fabrication of graphene nanoribbons with desired crystallographic orientations [17]. Thermo-chemical nano-lithography technique has also been presented as a promising SPN-AFM method [18].

Here we introduce a conceptually new approach to SPN, utilization of SPM with a rotating tip as an additional degree of freedom. Using atomistic modelling, density functional-based molecular dynamics simulations, and Fourier analysis we demonstrate this concept with the engineering of topological defects in a suspended graphene membrane, whereas the method is transferable to the larger class of two-dimensional (2D) materials. Defects have important roles in properties of graphene and other 2D materials [19, 20] hence large effort has been invested in understanding their effects, detection, elimination or utilization in engineering of desired materials' properties [21, 22]. Our simulations indicate that a choice of a material for the scanning probe tip, which does not strongly chemically interact with the graphene, allows rebinding of carbon atoms based primarily on positions of the atoms relative to nearest atomic neighbors of the tip. Rotation of the tip presents an additional degree of freedom to the standard SPM, which can provide a finer precision necessary to achieve desired relative positioning of tip and carbon neighbors. Note that one can rotate membrane rather than tip to achieve the same effect, since only relative positions matter. Application of STM on a rotating sample has already been experimentally

demonstrated [23]. In the second part of the manuscript we analyze possibility for engineering topological defects by the self-healing mechanism upon instant removal of the tip from the graphene membrane after the tip penetrated the membrane till certain depths. This approach can also be realized in an equivalent experiment with a similar effect, for example by irradiation of graphene membrane by energetic nanoscale clusters. The experimental feasibility to generate defects in graphene by this method but with supersonic microclusters has been recently demonstrated [24].

METHODS

We employ the density functional-based tight binding (DFTB) method [25, 26] as implemented in DFTB+ code [27]. The method has a proven record in research of plastic deformations of graphene, including our reports on breaking of graphene nanoribbons under extreme uniaxial stresses [28–30]. We perform geometry optimizations, molecular dynamics (MD) simulations and electronic transport calculations within Γ-point approximation. The initial geometries prior to MD simulations have been fully relaxed by the conjugate gradient optimization where maximal force on atoms is smaller than $0.04 \ eV/\text{Å}$. Van der Waals interaction has been included in calculations. Conductance of the systems is obtained by DFTB augmented by Green's functions [31] whereas the Landauer-Buttiker [32] formula is utilized for calculations of electronic current.

We investigate the mechanism of piercing of suspended graphene by atomically sharp STM tip within the supercell approach. The lengths of the supercell is 4.92 nm along the armchair direction of graphene and 5.11 nm along its zig-zag direction. The whole supercell contains 960 carbon (C) atoms and 120 gold (Au) atoms (Fig. 1(a)). The tip consists of face-centered cubic Au crystal with a pyramidal geometry. The tip apex is made of a single Au atom. The sides of the pyramid correspond to the stable Au(111) surfaces as shown in Fig. 1(a). Existence of pyramidal golden nanoclusters has been reported before [33]. We choose gold for the tip material since, as a noble metal, it does not strongly chemically interact with other materials including graphene. In order to isolate the effects of tip on graphene from eventual changes of tip geometry we do not allow Au atoms to relax during the simulations, essentially simulating an ideally rigid tip. The approximation is adequate for proving the concept while other weakly reactive tips, stronger than the target 2D material, should be utilized in real experiment.

RESULTS AND DISCUSSION

The drilling starts with the tip apex initially positioned above one of the three high-symmetry sites of graphene: the center of a phenyl ring (*hollow site*), on the top of a carbon atom (*top site*) or at the middle of a C-C bond (*bridge site*). The suspension of graphene is simulated by fixing C atoms that encompass two rows of phenyl rings at each edge of the simulated membrane. The starting position of the tip apex is 2Å above graphene. We optimize all initial geometries prior to MD simulations using the conjugate gradient method. The tip-graphene repulsion causes a shallow sag in graphene with maximal departure of C atoms by 1.01Å from the basal graphene plane (i.e. fixed C atoms).

After the initial geometry optimizations we proceed with MD simulations. The movement of tip is realized by alternating its translational motion inward graphene by 0.1Å and MD simulation with duration of 1 ps at the temperature of 300 K using the Nosé Hoover thermostat [34, 35]. This corresponds to the speed of 10 m/s, which is much smaller than speed of atoms due to their thermal motion. Hence effects of the tip kinematics can be neglected and the results of simulations are expected to be the same for much smaller tip velocities as the ones in real experiments. The depth z of tip apex relative to the graphene basal plane corresponds to the time t of MD simulations according to expression $z(t) = -2\text{Å} + 0.1\frac{\text{Å}}{ps}t$. We analyze the piercing mechanism for the three lateral tip positions. Two main regimes can be distinguished. After the initial elastic regime characterized by the parabolic-like dependence of potential energy with respect to time (equivalently the strain) the drilled graphene transits to the plastic regime with approximately linear dependence with abrupt discontinuities (Fig. 1(b,c,d)). The transitions from the elastic to the plastic regimes are triggered by the first breaking of chemical bonds in graphene during the piercing process. In case of the *hollow site* three alternative bonds of the phenyl ring under the tip apex break simultaneously (Fig. 1(b)). The system stabilization is twofold: (i) C atoms of the ring move away from the repulsive tip apex effectively lowering their mutual repulsion and (ii) three double bonds form which gain energy relative to the conjugated state of the stretched phenyl ring that existed prior the breakage of bonds. At the moment of breaking the angle between planes of that phenyl ring and neighboring rings is nearly 30°. When the tip apex is at the *top site*, the underneath C atom shifts faster than its three neighboring C atoms with the progress of tip (Fig. 1(c)). The corresponding three C-C bonds elongate until the threshold of 2Å is reached when two of the C-C bonds break simultaneously. The third bond contracts forming a shorter and stronger double or triple C-C bond. This rebinding releases energy, which transforms into the ki-
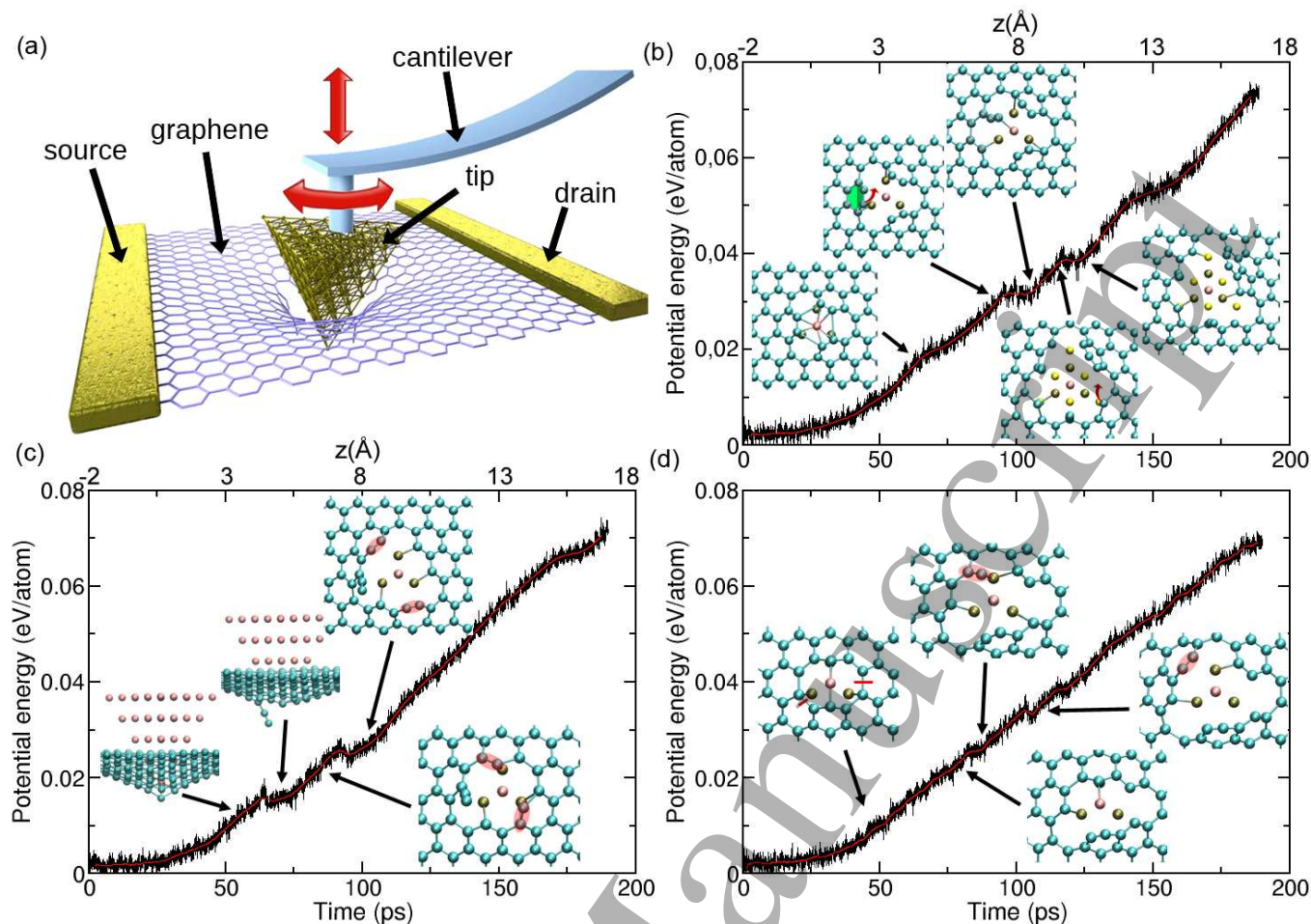
FIG. 1: (color online) Illustration of the scanning probe nanomanipulator with a rotating pyramidal golden tip is shown in panel (a). The surface area of the graphene membrane is around 5×5 nm. The suspension of graphene is realized in the MD simulations by fixing C atoms that encompass two rows of phenyl rings at each edge of the simulated membrane. Red arrows indicate translational and rotational degrees of freedom for the STM tip. Potential energy curves with respect to time of the tip progression (equivalently the depth z(Å) of tip apex relative to basal graphene plane) are shown for the *hollow, top* and *bridge* sites in panels (b), (c) and (d), respectively. These sites correspond to initial (i.e. at the first MD step) lateral positions of the tip apex above the center of a carbon hexagon (*hollow* site), above a carbon atom (*top* site) and above middle of a C-C bond (*bridge* site). The lateral position is fixed at the beginning of MD simulations and do not change as they progress. The structures in the panels (b), (c) and (d) are snapshots of MD simulations as viewed from a position below membranes. Red, golden and yellow spheres represent gold atoms of the tip apex, the second and third Au layers. Red lines and ellipses are eye guidance for bond breaking and bond rotations.

netic energy of the two C atoms. The energy is sufficient to tear off a C atom from the neighboring hexagon and a two-atom chain (i.e. a dimer) emerges (Fig. 1(c)). In case of the *bridge site* the bridge elongates with the penetration of the tip apex and breaks at the threshold bond length of 2Å (Fig. 1(d)). Breaking of the bond is not sufficient to transfer the released energy to a secondary relaxation as in the previous case. Interestingly, the initial change of the bonding in graphene, even so minor as that in the *bridge* case, changes the potential energy slope from the parabolic/elastic to the nearly linear/plastic. The potential energy has discontinuities in the plastic regime, each corresponding to certain stabilization mech-

anism and transformation of topology. Relative orientation of C atoms with their nearest Au neighbors and current local atomic structure of graphene primarily determine the mechanism of its structural reconfiguration. For example, around 100th picosecond the tip apex in the *hollow site* case has already passed through the graphene sheet whereas three Au atoms from the second tip layer are positioned next to certain C atoms (Fig. 1(b)). A phenyl ring bends (shown with green color in Fig. 1(b)) due to the proximity of the repulsive force of a neighboring Au atom. This causes the planar sp^2 hybridization to become unfavorable. One C-C bond of the ring breaks at the threshold bending angle of the ring of around $30°$ and
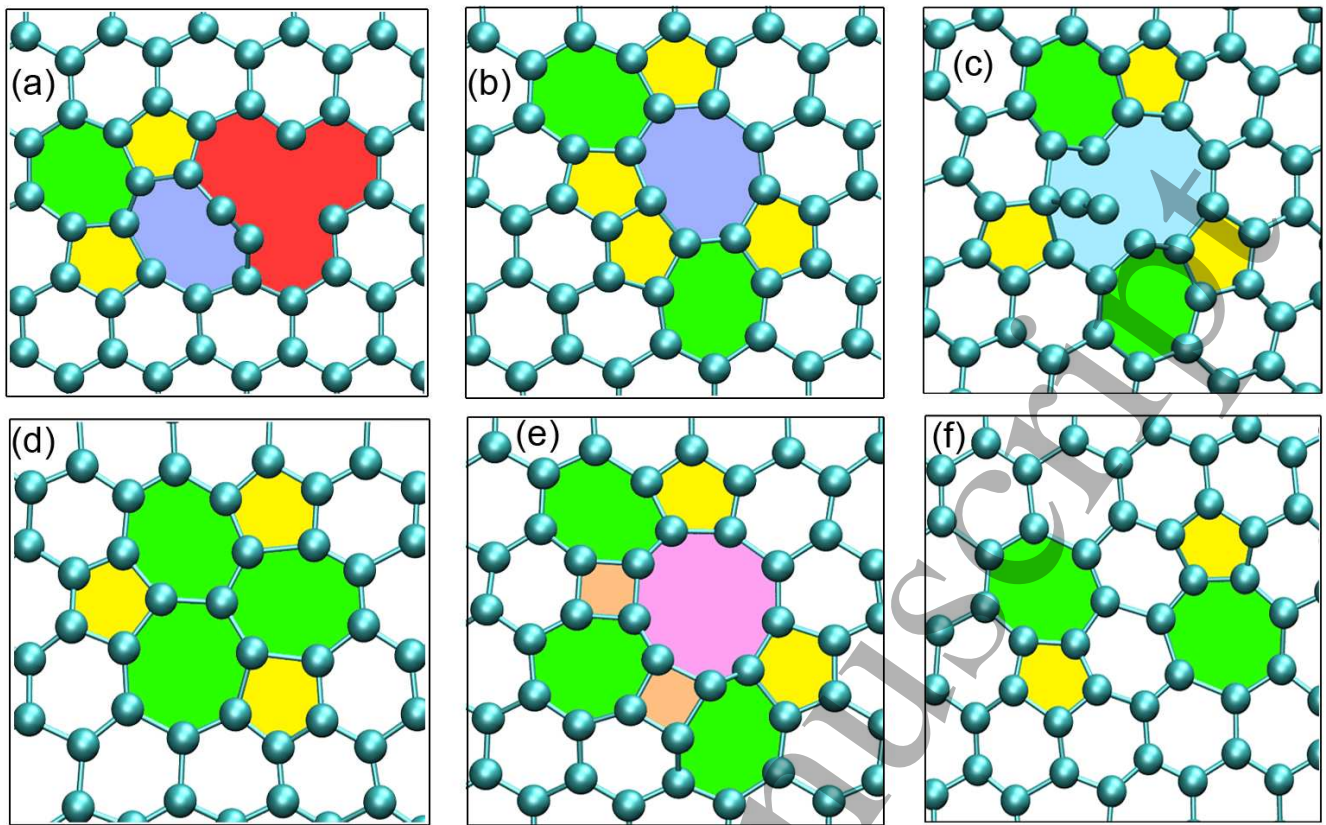
FIG. 2: (color online) Topological point defects obtained in the self-healing stage. The panels are referenced in Table I. Geometric figures (squares, pentagons, hexagons, etc.) are painted with different colors as eye guidance.

a two-atom chain forms, as indicated by the red arrow in Fig. 1(b). Due to the same atomic coordination, two additional C dimers form next to other two Au atoms from the second tip layer. In the *top site* case Au atoms from the second tip layer are nearly on top of two C atoms. A pair of C-C bonds, marked with the red ellipses in Fig. 1(c), rotate and form two heptagons. It is possible for a hexagon to accommodate an additional atom when the local strain is large enough such that more space is available for the atom. We observe the same process in the *bridge* case where the relative positions of Au and C atoms are close to those in the *top* case and a heptagonal ring also forms. The same interaction and reconfiguration mechanisms repeat when the 3rd Au layer arrives at the level of pores. For instance, in the *hollow site* case around 125th ps the third atomic layer of tip approaches graphene (represented by yellow spheres in Fig. 1(b)). When one of the Au atoms positions above a C atom in a zig-zag edge of the pore, the C atom moves into an empty space indicated by the red arrow, forming a pentagonal ring (Fig. 1(b)). In order to verify consistency of obtained results we have repeated segments of MD simulations starting 1ps before the simulation times when structural reconfigurations take over. In the repeated MD runs we shifted STM tip in random directions in the

basal plane of graphene by up to 0.5Å, prior continuation of the tip indentation. We have performed these simulations at only 300K for each C-C rebonding ten times. Surprisingly the same atomic structure reconfigurations are reproduced for all the cases. This indicates a comfortable margin for deterministic realization of real experiments at this and lower temperatures. We expect lesser reproducibility for higher temperatures. However, STM experiments can routinely be carried out even at much lower temperatures nowadays.

These findings of rather reproducible mechanisms for creation of atomic chains, pentagonal and heptagonal rings may be utilized for the controllable design and fabrication of topological defects in graphene. Since the reconfiguration of atomic bonds has been determined by the positions of Au atoms relative only to neighboring C atoms, rotation of the STM tip (red arrow in Fig. 1(a)) about axis perpendicular to basal plane of graphene, alternating with progression of tip through the membrane can position Au atoms at designated place for a desired reconfiguration to take over. The same mechanism continues in consequent retraction of tip from the membrane. Finally the membrane with aimed modification of atomic structure remains. Note that the intended relative positioning of tip and sample can be also achieved by rotating

TABLE I: Topological defects generated in the self-healing process

T(K)	Hollow			Top			Bridge		
	large	mid	small	large	mid	small	large	mid	small
50	(a)	(c)^a	6-gon	(c)	(c)	(c)	S-W	S-W	6-gon
300	(a)	(c)	6-gon	(c)	(b)	(c)	S-W	S-W	6-gon
600	S-W^b	(c)	6-gon	6-gon	(b)	S-W	S-W	6-gon	6-gon
900	S-W	S-W	6-gon	S-W	(b)	(c)	S-W	S-W	6-gon
1200	6-gon^c	S-W	6-gon	(e)^d	(d)	S-W	6-gon	S-W	6-gon
1500	S-W	6-gon	6-gon	6-gon	6-gon	6-gon	6-gon	(f)	6-gon
2000	S-W	(c)	6-gon	(d)	S-W	6-gon	6-gon	S-W	6-gon

* Large, mid and small indicate the size of initial pore before the relaxation stage; these correspond to removal of tip when tip apex is at depths of 17Å, 13Å and 8Å respectively.
** Letters in parentheses correspond to panels in Fig. 2;
^{a} Carbon chain like that in Fig.2(c) but with possible different configuration of surrounding atoms;
^{b} Stone-Wales defect;
^{c} Pristine hexagonal graphene;
^{d} A complex geometry with two C atoms driven out of graphene.

of sample instead of the tip, as experimentally demonstrated in ref. [23].

Next we analyze a relaxation mechanism of graphene membrane when STM tip is not retracted from graphene upon penetration but rather released beneath it. This is realized by simple removal of the tip at a given moment of MD simulation. The membrane starts to relax freely at that moment. We remove the tip at the 100th, 150th or 190th picosecond after the beginning of tip penetration. The corresponding initial sizes of the pores are designated as large, mid and small in the following text. The actual surface areas of the pores, difficult to precisely define due to their irregular nonplanar forms, range roughly from $40Å^2$ to $140Å^2$, which is from about 8 to 27 times larger than the surface of a phenyl ring in an unperturbed graphene membrane. We conduct MD simulations for a range of temperatures between 50 and 2000 K. These simulations are inspired by a recently reported experiment where graphene was penetrated by supersonic micrometer-sized atomic clusters [24]. This paper demonstrates a possibility to generate delocalized defects using this method. In contrast to the experiment our system is smaller by three orders of magnitude and cluster (i.e. tip) is significantly slower. The same method reported in the paper but with smaller and slower nanoclusters may be utilized for engineering of localized topological defects in graphene membranes.

Graphene self-heals within the first 1 ps of tip removal. The pores patch with new atomic structures presenting a variety of topological defects (see Fig. 2). Table I summarizes the fabricated structures for a range of temperatures, initial size of the pore and three initial puncturing sites, *hollow*, *top* and *bridge*, defined above. In contrast to controllable penetration and retraction of STM tip, atomic structures generated by the self-healing process are more nondeterministic. However some regularities are indicative of the MD simulations. The final atomic structure of the membrane is determined primarily by 3 factors:

- defects present in the system before the relaxation stage,

- breaking of bonds during relaxation and

- temperature.

The pristine hexagonal graphene is recovered for small initial pores in the *hollow* and *bridge* cases, whereas short carbon chains emerge for the *top* case, which reflect their atomic structures before the self-healing stage. Elastic energy of small pores accumulated in the puncturing phase is not sufficient to break a C-C bond during the self-healing process when edges of pores collide at each other. In contrast, a wide variety of defects emerges when pores are large (see Table I). Chemical bonds elongate with elevating temperatures, making 2D materials more flexible and their atoms more motile, essentially covering a larger part of phase space and possible number of atomic reconfigurations. Relatively high temperature and large pore with preexisting carbon chains is an optimal combination of conditions for fabrication of complex topological defects like the one in Fig. 2(e).

After the self-healing relaxation stage the accumulated strain energy localized around the pore transfers across the whole system via mechanical waves. We gain the information about the waves by the Fourier transform (FT) analysis. We obtain the power spectrum (Fig. 3(a)) of average depth of graphene for the *hexagonal site* case in the relaxation stage with respect to time (inset in Fig. 3(a)). The spectrum has the most pronounced peaks around 1.2 THz. The varying of heights of the peaks with temperature indicate damped waves with the characteristic
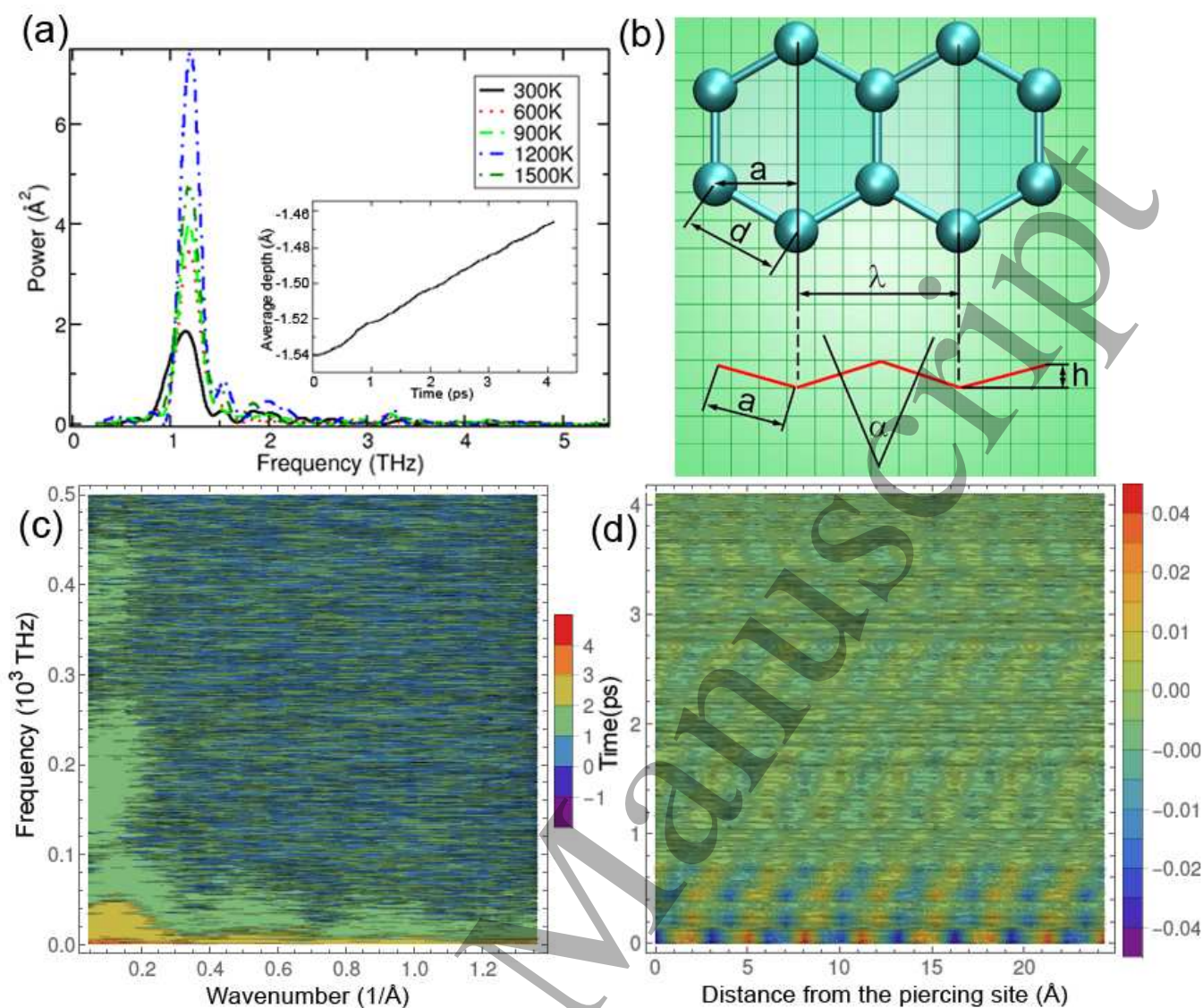
FIG. 3: (color online) (a) Fourier transform of average depth of graphene (average distance of C atoms from the basal plane of graphene) versus time (average depth dependence on time is shown in the inset). (b) Illustration of a mechanical wave with wavelength λ in graphene. Red line shows the side view where C atoms are alternatively shifted up and down. α is angle between planes shaded by dark and light green colors and h is twice the amplitude of the wave. (c) 2D Fourier transform from space-time to wavenumber-frequency domain. The legend scale is in dB. (d) Inverse 2D Fourier transform obtained from (c) for the optimal wavenumber 0.28 1/Å and all frequencies above 2.5 THz. The legend scale is given in Å.

attenuation time increasing with temperature. However the dependence is not monotonically increasing, as the highest peak is obtained for 1200 K rather than 1500 K. The origin of this anomaly is defect-dependency of attenuation, besides the temperature-dependency: while Stone-Wales defect emerges at 600, 900 and 1500 K the pristine defect-free graphene self-heals in simulation at 1200 K.

Now we analyze a possibility for secondary rupturing of graphene and eventual delocalization of defects due to the induced waves. We have observed above that carbon bonds break only under extreme dihedral an-

gles and bond lengths. In order to achieve such conditions with a wave, optimally its wave length has to be $\lambda = d\sqrt{3} = 3.46$Å for $d = 2$Å (bond length at which the C-C bond breaks), which corresponds to the wavenumber $k = 0.29$ 1/Å (Fig. 3(b)). The angle α between planes (marked with light and dark green shades) has to exceed $30°$. It follows that amplitude $h/2$ of the wave has to be around 0.27Å. We obtain amplitudes of induced waves from the space-time Fourier transform (STFT, Fig. 3(c)) and the inverse Fourier transform (IFT, Fig. 3(d)) for the optimal wavenumber $k = 0.29$ 1/Å after filtering out frequencies below 2.5THz. Periods of the filtered waves are
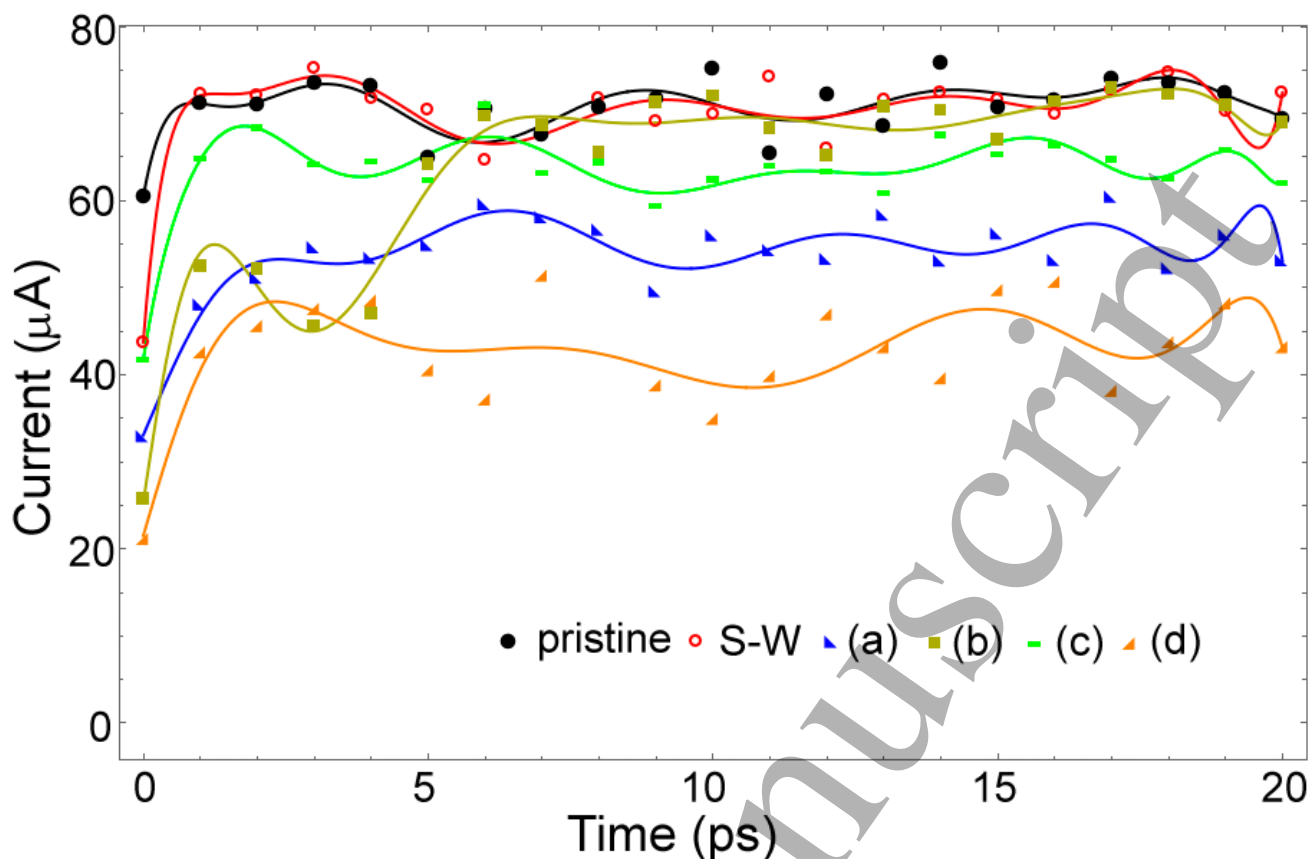
FIG. 4: (color online) Dependence of electronic current on time for systems with different defects. Zero time is at the beginning of self-healing process after removal of the SPM tip. Letters (a) - (d) in the legend correspond to defects in Fig. 2(b) - (d), and S-W to a single Stone-Wales defect. Chain is for the system shown in Fig. 2 (c) and pristine corresponds to self-healing to the ideal graphene. Various symbols designate actual values of calculated current whereas lines are polynomial fits to these values. Current is calculated for the bias voltage of 1V.

significantly large compared to the simulation time. The Fourier transforms are obtained for positions of atoms in a 1Å - wide stripe from the center of membrane to the extreme right position of the simulation box. Using this setup the STFT includes only one space coordinate along the stripe. We have interpolated the position of atoms prior to application of STFT. The power spectrum is the most prominent for small frequencies below $0.05 \cdot 10^3$ THz with relatively large fluctuations for higher frequencies. Note a propagating wave in Fig. 3(d) with the phase speed of around 280 m/s. Amplitude of the wave attenuates from 0.47 Å to below 0.05Å in only 0.7 ps. After that time the amplitude remains constant. Importantly, the amplitude of wave in the steady-state is significantly smaller than the threshold of 0.27 Å for the secondary breaking of carbon bonds. We have obtained the same conclusion for every considered temperature, puncturing site and initial size of pores. Therefore the topological defects remain localized around the penetration site since secondary defects can not emerge due to induced traveling waves. This finding may not be true

for another 2D materials, which stiffness is smaller than that of graphene as an extreme example.

Electronic transport of 2D materials sensitively depends on the nature of their defects. Fig. 4 shows the evolution of electronic current with time at bias voltage of 1V for investigated systems in the self-healing stage. Note that defects (a) to (d) in this section correspond to defects (a) to (d) in Fig. 2. Electrodes are placed at the opposite ends of membranes and consist of ideal graphene. All currents are calculated at 300K except for the case of defect (d), which is obtained at 1200K. The higher temperature causes a larger amplitude of oscillations of the membrane and correspondingly of electronic current. Defect (d) causes maximal degradation of conductance among investigated defects, by around 45% relative to the case of ideal graphene. It is followed with defects (a) and (c). A general feature is that currents are minimal at the beginning of the relaxation stage, when pores are still present in membranes. Electronic currents rapidly grow within the first 1 ps when the pores get closed and the final binding topology is reached for the

all defects. Current saturates to specific values depending on obtained defect, i.e. topology, while oscillating due to induced mechanical waves analyzed above in detail. While saturated currents are different for various defects ((a),(c) and (d)), our calculations also predict an unexpected overlapping of saturated currents in case of the pristine graphene, a single S-W and the (b) defect. The initial time dependence of current for these cases is still different, especially for the (b) defect. Therefore transport measurements of a defective graphene membrane during its self-healing process can provide information on specific topological defect fabricated in the membrane.

In conclusion, we have introduced a concept of SPM with a rotating tip as an additional degree of freedom. Our comprehensive MD simulations of puncturing of a suspended graphene membranes indicate a new possibility for engineering atomic structure of 2D materials in a controllable and reproducible manner with the novel SPM method. Another approach is releasing of the SPM tip after piercing of the membrane and its subsequent self-healing. The alternative to the latter method is shooting of membrane by a nanocluster. Although SPN looses a bit of determinacy when the latter approaches are used, fabrication a variety of individual topological defects is accessible. Additionally, Fourier analysis of oscillations induced by STM puncturing of graphene membrane indicate that generated defects remain local, i.e. they do not permeate off the puncturing site. The proposal for the new SPM method presented here and simulated on a suspended graphene membrane is a proof of concept, which can be applied to a wider range of two-dimensional materials. Manipulation of intrinsic atomic structure can be a qualitative step beyond the state-of-the-art of nanomanipulation today. The prior knowledge of tip geometry, details of its interaction with a 2D material and precise tip rotation by desired angles are the main challenges for successful experimental realization of the concepts presented here. All three challenges can be successfully addressed with present technologies or the sustained development of the technologies can reach the necessary level of sophistication. A controlled fabrication of atomically sharp STM tips has been in a steady progress during the years [36–38]. Atomistic simulations like these shown here can assist in gaining the details of the tip-sample interaction. The technique for controlling the rotational degree of freedom in SPM has been already demonstrated in ref. [23], where desired orientation of tip relative to sample is achieved by the rotation of sample instead of tip. These two approaches are equivalent, since only relative tip-sample orientation matters for fabrication of topological defects analyzed in our proposal. However a further improvement of the method is still necessary. Namely the circular scanning pattern shown in Ref. [23] has to be reduced to a rotation of sample with a fixed rotational axis that penetrates the tip apex.

The rotation axis should also be perpendicular to the membrane's basal plane for the sake of simplicity and better control of the tip-membrane interactions at the atomistic level. Hence, there are no physical obstacles that could principally forbid the realization of real experiments. The engineering issues that make real differences between somewhat idealized simulation conditions used here and realistic experiments will be resolved in the sustained progress of the field that we witness nowadays. Until then our concept and results can serve as a "thought experiment" without the complete overlap with current experimental possibilities, but as a guideline for their future development. In the meanwhile we can expect a realization of the second proposal here, engineering of the wide variety of the localized topological defects by nanocluster irradiation (the tip removal equivalence), for which the experimental techniques already exist. We hope the concept that we have presented will ignite a sufficient interest in the experimental community for the SPM with a rotating tip as a new tool for nanomanipulation, one of the ultimate goals in nanophysics and nanotechnology.

ACKNOWLEDGEMENT

---

* Electronic address: popov@ipb.ac.rs
[1] G. Binnig, H. Rohrer, C. Gerber, and E. Weibel, Appl. Phys. Lett. **40**, 178 (1982).
[2] G. Binnig, C. Quate, and C. Gerber, Phys. Rev. Lett. **56**, 930 (1986).
[3] D. Eigler and E. Schweizer, Nature **344**, 524 (1990).
[4] J. Lyding, T.-C. Shen, J. Hubacek, J. Tucker, and G. Abeln, Appl. Phys. Lett. **64**, 2010 (1994).
[5] M. Walsh and M. Hersam, Ann. Rev. Phys. Chem. **60**, 193 (2009).
[6] P. Sessi, J. Guest, M. Bode, and N. Guisinger, Nano Lett. **9**, 4343 (2009).
[7] J. Greenwood, T. H. Phan, Y. Fujita, Z. Li, O. Ivasenko, E. Vanderlinden, H. V. Gorp, W. Frederickx, G. Lu, K. Tahara, et al., ACS Nano **9**, 5520 (2015).
[8] J. Alaboson, C.-H. Sham, S. Kewalramani, J. Emery, J. Johns, A. Deshpande, T. Chien, M. Bedzyk, J. W. Elam, M. J. Pellin, et al., Nano Lett. **13**, 5763 (2013).
[9] J. E. Johns and M. Hersam, Acc. Chem. Res. **46**, 77 (2013).
[10] K. Mali, J. Greenwood, J. Adisoejoso, R. Phillipson, and D. Feyter, Nanoscale **7**, 1566 (2015).

[11] G.-Y. Liu, S. Xu, and Y. Qian, Acc. Chem. Res. **33**, 457 (2000).

[12] J. Dagata, J. Schneir, H. Harary, C. Evans, M. Postek, and J. Bennett, Appl. Phys. Lett. **56**, 2001 (1990).

[13] R. Garcia, R. Martinez, and J. Martinez, Chem. Soc. Rev. **35**, 29 (2006).

[14] A. Giesbers, U. Zeitler, S. Neubeck, F. Freitag, K. Novoselov, and J. Maan, Solid State Commun **147**, 366 (2008).

[15] L. Weng, L. Zhang, Y. Chen, and L. Rokhinson, Appl. Phys. Lett. **93**, 093107 (2008).

[16] S. Masubuchi, M. Ono, K. Yoshida, K. Hirakawa, and T. Machida, Appl. Phys. Lett. **94**, 082107 (2009).

[17] L. Tapasztó, G. Dobrik, P. Lambin, and L. P. Biró, Nature Nanotech. **3**, 397 (2008).

[18] Z. Wei, D. Wang, S. Kim, S.-Y. Kim, Y. Hu, M. K. Yakes, A. R. Laracuente, Z. Dai, S. R. Marder, C. Berger, et al., Science **328**, 1373 (2010).

[19] L. Liu, M. Qing, Y. Wang, and S. Chen, J. Mater. Sci. Tech. **31**, 599 (2015).

[20] F. Banhart, J. Kotakoski, and A. Krasheninnikov, ACS Nano **5**, 26 (2011).

[21] L. Vicarelli, S. Heerema, C. Dekker, and H. Zandbergen, ACS Nano **9**, 3428 (2015).

[22] D. Berger and C. Ratsch, Phys. Rev. B **93**, 235441 (2016).

[23] H. Nasrallah, P.-E. Mazeran, and O. Noël, Rev. Sci. Instrum. **82**, 113703 (2011).

[24] J.-H. Lee, P. E. Loya, J. Lou, and E. L. Thomas, Science **346**, 1092 (2014).

[25] D. Porezag, T. Frauenheim, T. Kohler, G. Seifert, and R. Kaschner, Phys. Rev. B **51**, 12947 (1995).

[26] G.Seifert, D. Porezag, and T. Frauenheim, Int. J. Quantum Chem. **58**, 185 (1996).

[27] B. Aradi, B. Hourahine, and T. Frauenheim, J. Phys. Chem. **111**, 5678 (2007).

[28] E. Erdogan, I. Popov, C. G. Rocha, G. Cuniberti, S. Roche, and G. Seifert, Phys. Rev. B **83**, 041401 (2011).

[29] E. Erdogan, I. Popov, and G. Seifert, Phys. Rev. B **83**, 245417 (2011).

[30] T. Kawai, M. Poetschke, Y. Miyamoto, C. Rocha, S. Roche, and G. Cuniberti, Phys. Rev. B **83**, 241405 (2011).

[31] V. Ivanovskaya, N. Ranjan, T. Heine, G. Merino, and G. Seifert, Small **1**, 399 (2005).

[32] S. Datta, *Electronic transport in mesoscopic systems* (Cambridge University Press, 1997).

[33] W. Huang, S. Bulusu, R. Pal, X. Zeng, and L. Wang, ACS Nano **3**, 1225 (2009).

[34] W. Hoover and B. Holian, Phys. Lett. A **211**, 253 (1996).

[35] S. Nosé, J. Chem. Phys. **81**, 511 (1984).

[36] A. Chaika, N. Orlova, V. Semenov, E. Postnova, S. Krasnikov, M. G. Lazarev, S. V. Chekmazov, V. Aristov, V. Glebovsky, S. Bozhko, et al., Sci. Rep. **4**, 3742 (2014).

[37] Z. Yu, C. Wang, Y. Du, S. Thevuthasan, and I. Lyubinetsky, Ultramicroscopy **108**, 873 (2008).

[38] J. Song, N. Pryds, K. Glejbøl, K. Mørch, A. Thølén, and L. Christensen, Rev. Sci. Instrum. **64**, 900 (1993).

Република Србија
Универзитет у Београду
Физички факултет
Д.Бр.2016/8019
Датум: 08.11.2017. године

На основу члана 161 Закона о општем управном поступку и службене евиденције издаје се

УВЕРЕЊЕ

Ђуришић (Вучина) Ивана, бр. индекса 2016/8019, рођена 30.08.1980. године, Беране, Црна Гора, уписана школске 2017/2018. године, у статусу: самофинансирање; тип студија: докторске академске студије; студијски програм: Физика.

Према Статуту факултета студије трају (број година): три.
Рок за завршетак студија: у двоструком трајању студија.

Ово се уверење може употребити за регулисање војне обавезе, издавање визе, права на дечији додатак, породичне пензије, инвалидског додатка, добијања здравствене књижице, легитимације за повлашћену вожњу и стипендије.

Овлашћено лице факултета

СРБИЈА И ЦРНА ГОРА

РЕПУБЛИКА СРБИЈА

ФИЗИЧКИ ФАКУЛТЕТ
УНИВЕРЗИТЕТА У БЕОГРАДУ

ДИПЛОМА

О СТЕЧЕНОМ ВИСОКОМ ОБРАЗОВАЊУ

Ђуришић Вучинћ Ивана

РОЂЕН-А 30-VIII-1980. ГОДИНЕ У БЕРАНАМА, БЕРАНЕ ЦРНА ГОРА , УПИСАН-А 2000/2001. ГОДИНЕ, А ДАНА 7. СЕПТЕМБРА 2005. ГОДИНЕ, ЗАВРШИО-ЛА ЈЕ СТУДИЈЕ НА ФИЗИЧКОМ ФАКУЛТЕТУ УНИВЕРЗИТЕТА У БЕОГРАДУ, НА СТУДИЈСКОЈ ГРУПИ ФИЗИКА СА ОПШТИМ УСПЕХОМ 9,07. (ДЕВЕТ И 07/100) У ТОКУ СТУДИЈА И ОЦЕНОМ 10 (ДЕСЕТ) НА ДИПЛОМСКОМ ИСПИТУ

НА ОСНОВУ ТОГА ИЗДАЈЕ МУ-ЈОЈ СЕ ОВА ДИПЛОМА О СТЕЧЕНОМ ВИСОКОМ ОБРАЗОВАЊУ И СТРУЧНОМ НАЗИВУ

ДИПЛОМИРАНИ ФИЗИЧАР

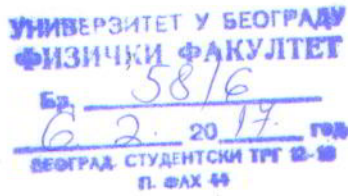РЕДНИ БРОЈ ИЗ ЕВИДЕНЦИЈЕ О ИЗДАТИМ ДИПЛОМАМА 2252005

У БЕОГРАДУ 14–IX–2005.   ГОДИНЕ

ДЕКАН

проф.др Снежана Прндаревић

РЕКТОР

проф.др Дејан Поповић

УНИВЕРЗИТЕТ У БЕОГРАДУ
ФИЗИЧКИ ФАКУЛТЕТ
Бр. 5876
6 2 20 17 год.
БЕОГРАД, СТУДЕНТСКИ ТРГ 12-16
П. ФАХ 44

ПОТВРДА

Овим се потврђује да је ИВАНА ЂУРИШИЋ, дипломирани физичар, пријавила Наставно-научном већу Физичког факултета докторску дисертацију под називом: „ЕЛЕКТРОНСКЕ И ТРАНСПОРТНЕ ОСОБИНЕ НУКЛЕИНСКИХ КИСЕЛИНА".

Наставно-научно веће Физичког факултета, на својој седници одржаној 30. јануара 2013. године прихватило је предложену тему и за ментора одредило др Радомира Жикића, вишег научног сарадника Института за физику.

Веће научних области природно-математичких наука Универзитета у Београду, на својој седници одржаној 25. фебруара 2013. године прихватило је предложену тему и одобрило рад на докторској дисертацији.

Београд, 6.2.2017.

ДЕКАН ФИЗИЧКОГ ФАКУЛТЕТА

Проф. др Јаблан Дојчиловић